PHYSICAL REVIEW B VOLUME 28, NUMBER 11 1 DECEMBER 1983

X-ray scattering study of the structure and freezing transition of monolayer xenon on graphite

P. A. Heiney,* P. W. Stephens,† and R. J. Birgeneau
Department of Physics and Research Lab of Electronics, Massachusetts Institute of Technology, Cambridge, Massachusetts 02139

P. M. Horn
IBM Thomas J. Watson Research Center, Yorktown Heights, New York 10598

D. E. Moncton‡
Bell Laboratories, Murray Hill, New Jersey 07974
(Received 20 July 1983)

We have performed an extensive x-ray scattering study of the freezing transition of incommensurate xenon physisorbed on graphite as a function of temperature and chemical potential. At a coverage of 1.1 monolayers the transition is continuous to within the substrate-determined resolution, with correlation lengths in the fluid phase exceeding 50 atomic spacings. At coverages less than one monolayer the transition is first order. A comparison is made with current theories of two-dimensional melting.

I. INTRODUCTION

The last 15 years have seen intensive research on the structure, thermodynamics, and phase transitions of simple gases adsorbed on graphite.[1–4] The behavior of both rare gases such as krypton and xenon, and more complicated molecules such as oxygen and methane, have been studied using a number of techniques including adsorption isotherms, heat capacity, x-ray scattering, low-energy electron diffraction (LEED), and neutron scattering. Exfoliated graphites such as Union Carbide Grafoil and *ZYX* have proved exceptionally useful as substrates because of their large, relatively homogeneous surfaces.[5] We have used high-resolution x-ray scattering to study the melting transition of xenon adsorbed on *ZYX* exfoliated graphite as a function of both temperature and coverage near monolayer density. These experiments were motivated in part by theoretical and numerical studies which made varying predictions about the nature of the two-dimensional (2D) melting transition, some predicting a first-order transition and others predicting a continuous transition with unusual properties. Xenon forms a triangular 2D lattice that is incommensurate with the graphite substrate at temperatures near the melting transition, and both the adatom-adatom and adatom-substrate interactions approximate simple Lennard-Jones potentials. It therefore provides a particularly good experimental realization of an ideal 2D solid. We find that in the submonolayer regime, the melting transition is strongly first order, but that at coverages greater than one monolayer the melting transition appears to be continuous.

In Sec. II we summarize briefly current theoretical work on the melting transition of 2D solids. Section III reviews previous work on the xenon on graphite system. In Sec. IV we describe the experimental techniques used, and in Sec. V we describe the data analysis. Section VI describes high-resolution x-ray data taken at the Stanford Synchrotron Radiation Laboratory (SSRL), while Sec. VII describes more extensive but lower-resolution data measured with a rotating-anode x-ray generator at the Massachusetts Institute of Technology (MIT). In Sec. VIII we discuss our results and compare them with the theoretical predictions.

II. REVIEW OF THEORY

It has been known for 50 years[6–12] that true crystalline long-range order (LRO) is impossible in a 2D solid. At finite temperatures the divergent long-wavelength fluctuations convert the zero-temperature δ function diffraction peaks at reciprocal-lattice points $\vec{\tau}$ to power-law singularities[13–15] of the form

$$S(\vec{Q}-\vec{\tau}) \propto |\vec{Q}-\vec{\tau}|^{\eta_\tau-2}, \quad \eta_\tau=\frac{k_B T \tau^2}{2\pi\rho c^2}, \tag{1}$$

where c is the speed of sound and ρ is the mass density. In this low-temperature phase long-range bond-orientational order survives. A physically appealing theory originally developed by Berezinskii[16] and Kosterlitz and Thouless[17] predicts that 2D systems with two degrees of freedom may have a continuous disordering transition mediated by the thermal unbinding of topological defects (dislocations in the case of crystals). At high temperatures a phase transition can take place to a disordered phase, which is characterized by exponential decay of both orientational and positional order. The presence of a substrate has interesting consequences. If the substrate is commensurate with the 2D lattice, long-range positional order can be restored. For incommensurate substrates, as in the present case of xenon on graphite, the long-

wavelength phonons of the 2D lattice will still produce a power-law structure factor. However, Novaco and McTague[18] have shown that the ground-state energy of an incommensurate 2D crystal is minimized when its crystalline axes have a definite orientation with respect to the substrate ("orientational epitaxy"). Thus the chief effect of the substrate is to provide an orientation field which will impose some degree of bond-orientational order even in the completely disordered phase.

Nelson, Halperin, and Young[19,20] have developed a dislocation-mediated melting theory in detail for the case of a triangular solid on a substrate which provides an orienting field but does not influence the long-range positional order. This appears to be an appropriate model for xenon on graphite. A novel prediction of this theory is that the melting will proceed in two stages: Above the melting temperature T_c the adsorbed layer will have exponentially decaying positional correlations but will retain a power-law decay in bond-orientation correlations. This novel intermediate state is called the "hexatic" phase. Above a higher temperature T_i, both positional and orientational order are short range. The Kosterlitz-Thouless-Halperin-Nelson-Young (KTHNY) theory makes a number of explicit predictions for the critical behavior near T_c. The correlation length on the fluid side of the transition diverges exponentially,

$$\xi_+ \propto \exp\left[B\left(\frac{T_c}{T-T_c}\right)^{\nu}\right], \tag{2}$$

where $0.3696\ldots<\nu<0.4$. The exponent describing the (1,0) peak is restricted to the range

$$\tfrac{1}{4} \leq \eta_{(1,0)}(\text{melting}) \leq \tfrac{1}{3}\ . \tag{3}$$

As T approaches T_c from above, $S(\vec{\tau})$ diverges with

$$S(\vec{\tau}) \propto [\xi_+(T)]^{2-\eta_\tau}\ . \tag{4}$$

Equally detailed predictions were made for the hexatic-to-liquid transition, but since our experiments did not address the existence of the hexatic phase these predictions will not be discussed here.

The KTHNY model assumes a continuous transition and develops a self-consistent theory based on the unbinding of thermal dislocations. It is always possible that some other mechanism, such as the spontaneous formation of grain boundaries, might cause a first-order transition at a lower temperature. There have been a number of other theories of 2D melting, most employing a mean-field approach, many of which predict a first-order transition.[21–27]

A considerable number of molecular dynamics and Monte Carlo calculations have been done on the 2D melting problem, based on a wide variety of potentials (power law, hard sphere, Lennard-Jones, and Gaussian).[28–47] The results have proven to be controversial, with some authors seeing behavior consistent with the KTHNY picture, some seeing evidence for a first-order transition, and some[39] claiming that both types of transition are possible. Computer simulations are typically done using no more than several thousand particles, and sampling no more than several million configurations, which corresponds to a very short interval on a "real" time scale.[48] This means that continuous transitions, which typically involve large fluctuations and critical slowing down, may be confused with first-order transitions which show coexistence and hysteresis. It may, in fact, be very difficult to determine the nature of a transition on the basis of numerical calculations. On the other hand, computer studies have the advantage that local atomic arrangements can be studied directly. A recent computer simulation by Abraham,[31] which incorporates the possibility of promotion to a second layer and models the xenon-graphite interactions as closely as possible, yields results which are similar to our diffraction results, although his interpretation is somewhat different. Specifically, he regards fluctuations of the number of particles in the first layer as signifying an inherent instability in the overfilled xenon monolayer. In the experimental case, the presence of the three-dimensional (3D) vapor means that the film is described by a grand-canonical ensemble, for which local fluctuations of the number of adsorbed particles are to be expected, particularly near a second-order phase transition. Furthermore, because one cannot distinguish the separate layers as distinct phases, the exchange of atoms between layers does not imply the presence of more than one phase.

III. PREVIOUS EXPERIMENTAL STUDIES

The bulk properties of xenon are well known.[49–51] Bulk solid xenon has the fcc structure with a nearest-neighbor distance of 5.31 Å. The critical-point and triple-point temperatures and pressures are the following: $T_{3c}=389.7$ K, $p_{3c}=57.64$ atm, $T_{3t}=161.3$ K, and $p_{3t}=612$ Torr. The Debye temperature of the solid is approximately 64 K.

Although the adsorption of xenon on graphite has been studied since 1957,[52–55] the first clear evidence for phase transitions in physisorbed xenon on graphite was seen in 1966 with the pioneering LEED experiments of Lander and Morrison.[56] At $T=90$ K, $P\sim10^{-3}$ Torr, Lander and Morrison saw a LEED pattern that they attributed to a $\sqrt{3}\times\sqrt{3}\ R\,30°$ commensurate structure. It is now believed that the structure they observed was incommensurate, but too close to the epitaxial spacing for them to resolve the difference. Heating the sample a few degrees caused the adsorbed xenon crystal to melt. The first isotherm measurements for xenon on exfoliated graphite were performed by Thomy, Duval, and co-workers.[57,58] From detailed isotherm measurements, they constructed the phase diagrams for Xe and other gases adsorbed on graphite. The phase diagram of submonolayer xenon (see Figs. 1 and 2) is similar to that of 3D xenon, with distinct gas, liquid, and solid phases. The two-dimensional (2D) Xe triple-point and critical-point temperatures were measured to be $T_{2t}=99$ K and $T_{2c}=117$ K. Suzanne and *et al.*[59] and Bienfait and Venables[60] performed LEED and Auger studies which confirmed and extended the Thomy and Duval results in the low-pressure regime and provided

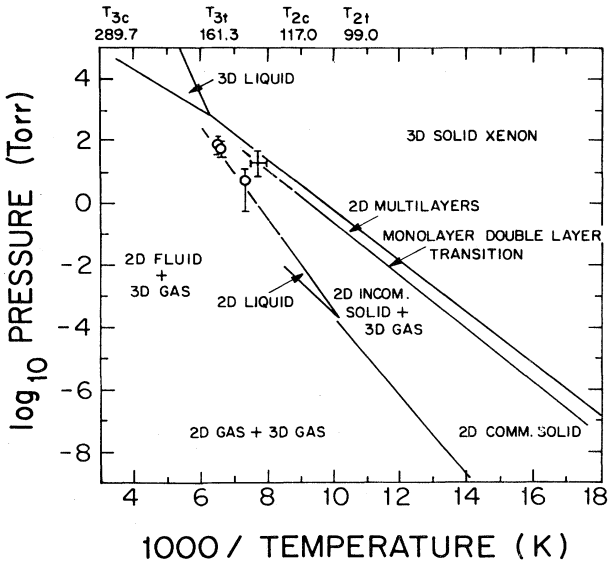

FIG. 1. Phase diagram of xenon in the presence of a graphite substrate. Solid lines are from Refs. 49—51, 57—60, and 66, dashed lines and circles are new results.

information about atomic vibrations and growth kinetics in the submonolayer regime. Venables *et al.*[61] performed a series of electron-diffraction experiments which showed for the first time that Xe has a low-temperature commensurate-incommensurate transition, and is incommensurate for all temperatures in the vicinity of the triple point. They also observed the orientational epitaxy of incommensurate 2D Xe solids. Using ellipsometry, Quentel *et al.*[62] were able to confirm independently the isotherm results of Thomy and Duval. Ellis *et al.*[63] have diffracted hydrogen atoms from xenon adsorbed on graphite, and report that at 26 K, Xe/graphite forms the $\sqrt{3}\times\sqrt{3}\,R\,30^\circ$ commensurate structure. Litzinger and Stewart[64] performed heat-capacity measurements in the coverage-temperature region $0.19\leq\Theta\leq1.05$, $65\leq T\leq160$ K. (The coverage Θ is in units of one monolayer.) The presence of a constant-temperature line of anomalies between $0.2\leq\Theta\leq0.7$ at $T=99.95$ K confirms the existence of a submonolayer triple point. The heat-capacity peak becomes unmeasurably weak at higher coverages.

Brady, Fein, and Steele[65] performed x-ray scattering measurements of xenon on spheron (a form of carbon black) but since they took data only in the region $0.1\leq\Theta\leq1.05$, $T=175$ K, they only observed scattering from a 2D fluid. Hammonds *et al.*[66] performed x-ray scattering experiments in the region $0.30\leq\Theta\leq2.0$, $88\leq T\leq112$ K. This work confirmed the isotherm results of Thomy and Duval and the LEED result of Lander and Morrison in detail, including the identification of a 2D triple point at 99 K. The 2D solid phase at $T=112$ K was found to be triangular and incommensurate. The evolution of peak intensity with coverage showed that successive layers form an hcp or fcc stacking pattern. This result is consistent with the observation that the 2D xenon lattice constant very nearly matches the nearest-neighbor distance in the (111) planes of 3D fcc solid xenon. Some of the x-ray results on monolayer xenon melting described in this paper have been reported elsewhere.[67]

Other studies of the melting of incommensurate physisorbed phases have been performed on CD_4 (Ref. 68) and argon.[69] The methane data were analyzed using similar techniques, and yielded results consistent with, the present work, showing evidence of a continuous melting transition in monolayer adsorbed methane. This experiment was

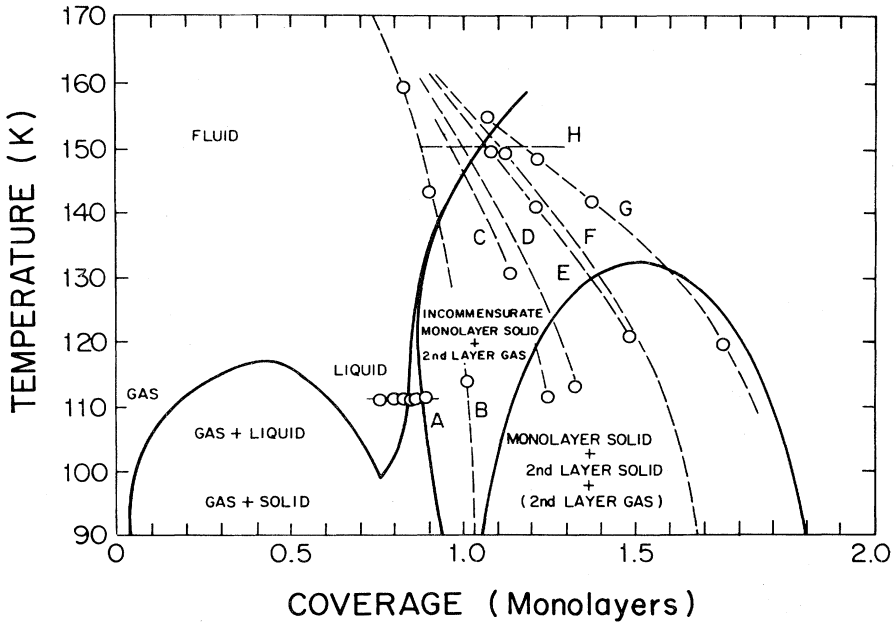

FIG. 2. Phase diagram of xenon on graphite between 0 and 2 monolayers. Dashed lines are paths followed in experiments. *A*, SSRL III; *B*, MIT1.01; *C*, MIT1.26; *D*, MIT1.33; *E*, MIT1.57; *F*, MIT1.59 and SSRL I; *G*, MIT1.84; *H*, SSRL II.

carried out with a resolution somewhat lower than that of the rotating-anode data described in Sec. VIII, and was therefore unable in our opinion to differentiate unambiguously between power-law and exponential correlation functions for correlation lengths exceeding about 40 Å. The purpose of the argon experiment was to make a systematic comparison between the phase diagrams of argon, krypton, and xenon adsorbed on *ZYX* exfoliated graphite. The melting transition of argon was studied with high-resolution synchrotron techniques ($L_{\text{eff}}=1200$ Å) and was found to be continuous at higher densities. The signal level in the present work was sufficiently high to enable a more detailed analysis of the data than was possible in the argon experiment. Further experiments on the argon-on-graphite system by the same group and two of us (P.W.S. and D.E.M.) using a higher-flux wiggler beam line at SSRL are currently in progress. Dimon *et al.*[70] have recently performed measurements which confirm our identification of a tricritical point at $T\sim 125$ K, to be discussed below. Rosenbaum *et al.*[71] have recently performed a scattering measurement of xenon on single-crystal—exfoliated graphite; their measurements support the Nelson-Halperin prediction of a hexatic phase.

The p-T projection of the Xe/graphite system is shown in Fig. 1. The 2D triple-point and critical-point temperatures are at approximately 0.4 times their bulk values. The 2D solid-fluid phase boundary and the 3D liquid-gas phase boundary are observed to converge. Since symmetry considerations argue against the existence of a monolayer critical point, the monolayer liquid-solid phase boundary must terminate either at a multilayer phase boundary or at the bulk liquid-gas phase boundary. The corresponding Θ-T projection of the Xe/graphite phase diagram is shown in Fig. 2. Below $T=99$ K and $\Theta=1$ the only possible phases are a dilute gas or a monolayer solid containing a small number of vacancies. A broad first-order coexistence region separates these two phases. There is a triple point at 99 K, above which the system makes first-order transitions between a dilute gas, a dense liquid, and a monolayer solid. At $T=112$ K, the solid-fluid coexistence region is quite narrow, with boundaries at $0.84\leq\Theta\leq 0.88$. At $T=117$ K and $\Theta=0.4$ there is a critical point above which the only phases are a fluid and a monolayer solid.

The monolayer solid has a triangular structure that is incommensurate with the substrate at all coverages measured when $T>70$ K. However, as will be discussed below, the position of the solid Xe(1,0) peak near the melting transition was found to be close to $\tau=1.60$ Å^{-1}, only 6% away from the $\sqrt{3}\times\sqrt{3}\,R\,30°$ commensurate value $\tau_{\text{comm}}=1.70$ Å^{-1}. In thermal equilibrium, the monolayer solid must have both atoms promoted to the second layer and vacancies in the first layer. Increasing coverage forces the crystal to contract and promote atoms to the second layer. At $T=112$ K, the (1,0) reciprocal-lattice position increases continuously with increasing coverage, reaching a limiting value $\tau=1.64$ Å^{-1} at $\Theta=1.5$. On the other hand, the reciprocal-lattice vector at the coexistence-region boundary is $\tau=1.59$ Å^{-1}. If we assume that $\tau=1.64$ Å^{-1} corresponds to a completely filled first-layer solid with no vacancies, and that at the coexistence boundary there are no second-layer atoms, we find that the coverage at $\Theta=0.88$, $T=112$ K is $0.88\times(1.64/1.59)^2=0.94$ in "expanded" lattice units. This means that the submonolayer xenon solid can support at least 6% vacancies before melting.

Two features are apparent in the region between $\Theta=1$ and 2. Firstly, there is a region of coexistence between a monolayer solid with second-layer gas and a two-layer solid. While it is plausible that such a region must exist, the exact phase boundaries above $T=112$ K are not known. Secondly, the narrowing of the solid-fluid coexistence region has been extrapolated to a multicritical point above which the transition is continuous. As will be discussed in more detail below, the liquid-solid transition is almost certainly first order at $T=112$ K and continuous at $T=150$ K. The exact location of the supposed multicritical point is bracketed between these two values.

IV. EXPERIMENTAL METHOD

Two sets of measurements were performed: A series of three high-resolution experiments using synchrotron radiation at SSRL, and a more complete, but much lower-resolution set of measurements done using a rotating-anode x-ray generator at MIT. The two sets of experiments employed different samples, sample cells, gas-handling equipment, and diffractometers, but were similar in many respects. The MIT data were obtained first, but were reanalyzed when the much-higher-quality SSRL data became available. Many of the experimental details have been described elsewhere.[5,66,76]

Both sets of experiments used Union Carbide UCAR-*ZYX* exfoliated graphite.[72] The properties of UCAR-*ZYX* have been discussed elsewhere[5]; it has preferentially oriented adsorption surfaces, a surface coherence length $L=2000\pm 300$ Å, and a specific surface area $1-3$ m^2/g. The distribution of planar orientations is approximately Gaussian with a halfwidth at half maximum (HWHM) of $\sim 11°$. The SSRL sample measured $12\times 12\times 2$ mm^3, with the c axis parallel to the thin direction. Only the center 20 mm^3 were exposed to x rays. The MIT sample was cut into strips measuring $24\times 2.5\times 1$ mm^3. The strips were drilled and threaded onto thin rods, with the c-axis vertical, to form a sample with dimensions $24\times 22\times 2.5$ mm^3. In the MIT configuration the sample was rotated about the c axis, while in the SSRL configuration the c axis was in the plane of scattering, but in both cases the momentum-transfer wave vector $\vec{k}=\vec{k}_f-\vec{k}_i$ was in a basal-plane direction, and perpendicular to the c axis. Sample thicknesses in the range 1—2 mm are convenient since the x-ray attenuation depth at $\lambda=1.5$ Å of *ZYX* graphite is ~ 1 mm. The graphite was prepared by baking it at 900 °C under a vacuum $\leq 10^{-5}$ Torr for several hours to remove contaminants and loading it into the sample cell under clean nitrogen atmosphere.

The SSRL sample cell was constructed of aluminum, with cylindrical beryllium windows. It was approximately 25 mm high and 20 mm in diameter. The rectangular

MIT sample cell was constructed of stainless steel with flat beryllium windows. The inside dimensions were $26\times24\times4.2$ mm.[3] Temperature control was maintained using Air Products Displex cryostats with platinum resistance and silicon diode thermometers. The sample temperature was measured with a precision of 0.01 K and an absolute accuracy of 0.5 K. The amount of gas adsorbed on the graphite surface was measured volumetrically; pressures were measured using two Baratron pressure gauges with full scale ranges $10^{-4}-10$ Torr and $10^{-2}-10^{3}$ Torr, respectively (1 Torr=1 mm Hg), and were corrected for thermal transpiration.[73] The experimentally measured units of surface coverage were (change in pressure)$\times$(dosing volume) at room temperature; the equivalent fractional surface coverage was calculated indirectly from adsorption isotherms and measured structural changes. Both the position of inflection points in the xenon adsorption isotherm[57,74] and the measured coverage at the krypton commensurate-incommensurate transition yield an adsorbed volume of 560 ± 30 Torr cm^3 ($=1.8\times10^{19}$ atoms) at monolayer coverage for the MIT sample and 97 ± 5 Torr cm^3 for the SSRL sample.

The MIT measurements were all done in a "closed-cell" configuration in which a fixed amount of gas was let into the sample cell, which was then sealed off. In this type of scan, the surfaces coverage changes slightly with temperature because of gas exchange with the 3D gas in the dead volume of the cell. At a few temperatures the cell was opened and the vapor pressure measured; the path through the phase diagram was interpolated between these measured points, which are indicated with open circles in Fig. 2. The closed-cell technique was used to minimize impurity contamination by the gas-handling system, since each run lasted for several days. Scans done in this way will henceforth be labeled MITx, where x is the amount of gas in the cell measured in coverage units, i.e., MIT1.59 refers to an experiment in which an amount of xenon corresponding to 1.59 monolayers was sealed in the cell. This represents the true surface coverage only at zero temperature.

The SSRL measurements were done three different ways. SSRL I was a closed-cell scan at a fractional dosage very close to that of the MIT1.59 run; the vapor pressure at $T=150$ K was 50.0 Torr as compared with 48.03 Torr at $T=149.25$ K in the MIT1.59 run. The SSRL II run was done as a function of vapor pressure at a constant temperature $T=150.0$ K; it crossed the liquid-solid phase boundary at approximately the same point as the MIT1.59 and SSRL I runs (1.1 monolayers). The SSRL III run was done as a function of surface coverage at a constant temperature $T=112$ K.

The paths of the various MIT and SSRL runs are shown in dashed lines in Fig. 2. There is an important difference between closed-cell scans done as a function of temperature and constant-temperature scans done as a function of 3D vapor pressure (i.e., chemical potential): A closed-cell scan steps through a first-order coexistence region, whereas a chemical-potential scan jumps over such a region. Both types of scan follow similar paths across a continuous transition line. In all cases mass exchange took place not only between the adlayer and the 3D vapor but also between the filled first layer and the partially filled second layer. The xenon-graphite system is 2D only in the sense that solid correlations only develop parallel to the graphite planes.

The high-resolution experiments used the synchrotron radiation from the eight-pole wiggler at Beamline VII of SSRL.[75] The x rays were focused by a metal-coated mirror. The beam was monochromated by a double Si(111) monochromator tuned to $\lambda=1.74$ Å, passed through a monitor and slits, diffracted from the sample in the vertical direction, diffracted from a Ge(111) analyzer crystal, and measured by a NaI scintillation detector. Scattering was done in transmission in an essentially nondispersive configuration. The longitudinal resolution was $\Delta q=0.0003$ Å^{-1} HWHM. This was considerably narrower than the sharpest Xe(1,0) peak, which had a finite-size-determined width of 0.0016 Å^{-1} HWHM. The out-of-plane resolution was $\sim1°$ HWHM.

The source of the x rays in the low-resolution experiments was a Rigaku 12-kW rotating-anode x-ray generator operating at 8 kW. The scattering was done in transmission in a two-axis configuration. The monochromator was a 1×1 in.^{2} vertically focusing graphite (002) monochromator, which selected the Cu $K\alpha$ spectral line ($\lambda=1.5418$ Å). The beam was further collimated by slits before and after the monochromator and immediately before the sample, and by Soller slits in front of the scintillation detector. The longitudinal instrumental resolution was $\Delta q=0.0085$ Å^{-1} HWHM, corresponding to a real-space resolution $\pi/\Delta q=370$ Å. The out-of-plane resolution was approximately 2° HWHM. Both diffractometers were controlled by PDP 11/34 minicomputers via "computer automated measurement and control" (CAMAC) instrumentation interfaces.

V. DATA REDUCTION

We now discuss the data analysis, some details of which have been described elsewhere.[76] The scattered x-ray intensity was normalized to the monitor signal. The resultant intensity was compared via least-squares fits to various theoretical models. A least-squares fit yields a goodness-of-fit parameter χ^2, which represents the average deviation of the model from the data in units of one standard deviation. It is important to note that the value of χ^2 thus obtained depends on the counting statistics. In the limit of very poor statistics, the standard error is large, and χ^2 is not highly sensitive to the model used. As the counting statistics improve, χ^2 will increase for incorrect models but will remain close to unity for the correct model in the absence of systematic experimental errors.

As discussed in Sec. II, it is expected that in a true 2D solid the δ-function Bragg peaks will be replaced by power-law singularities of the form [Eq. (1)]. In a 2D fluid the scattering take the form of broad cylindrical tubes. In a 2D orientationally ordered or hexatic fluid we expect that Ornstein-Zernike decay of real-space correlations will lead to a Lorentzian in-plane scattering cross section

$$S(\vec{Q}) \propto \frac{1}{(\vec{Q}-\vec{\tau})^2+\kappa^2} . \tag{5}$$

It was found that crystalline peaks were in fact also well modeled by sufficiently sharp Lorentzians, although this is unphysical; this effect will be discussed in detail later. These intrinsic scattering cross sections are modified by a number of factors to give the measured signal. Both the instrumental resolution and finite-sample-size effects smooth out the power-law singularity in the solid line shape and also broaden a Lorentzian line shape. Indeed, the instrumental resolution and finite-size rounding affect the line shape the same way. If one neglects the finite-size cutoff of low-frequency phonons, the instrumental resolution and the finite-size effect both contribute Gaussian terms to the peak width. Thus, the instrumental broadening can be incorporated in an effective finite sample size

$$L_{\text{eff}}=[L^2+(\pi/\delta)^2]^{1/2} , \tag{6}$$

where L is the intrinsic sample size and δ is the instrumental width. Several approximate formulas for a power-law line shape convoluted with finite-size rounding have been published[77,78]; we have used the approximation of Dutta and Sinha,[78]

$$S(q)=\left[\frac{L}{a}\right]^{2-\eta}\left[\frac{2}{\gamma\sqrt{\pi}}\right]^{\eta}\Gamma\left[1-\frac{\eta}{2}\right]\Phi\left[1-\frac{\eta}{2};1;-\frac{q^2 L_{\text{eff}}{}^2}{4\pi}\right] ,$$
$$\Phi(b;c;z)=\sum_{s=0}^{\infty}\frac{\Gamma(b+s)\Gamma(c)z^s}{\Gamma(b)\Gamma(c+s)s!} , \vec{q}=\vec{Q}-\vec{\tau} , \quad \gamma=1.781\,024\cdots , \tag{7}$$

where Φ is the degenerate hyperbolic function ("Kummer's function"). $\Phi(b;c;z)$ is well behaved for small z, but contains a large number of oscillatory terms when $|z|$ is large. Therefore, for $z \geq 10$, an alternate expression was used,[79]

$$\Phi(a;b;z)=e^z\Phi(b-a;b;-z) ,$$
$$\Phi(a;b;z)\approx\frac{\Gamma(b)}{\Gamma(b-a)}z^{-a}, \quad |z| \gg 1 . \tag{8}$$

Note that the forms [Eqs. (7) and (8)] are universal functions of qL_{eff}. It is straightforward to verify that this line shape becomes a finite-size Gaussian in the limit $qL_{\text{eff}} \ll 1$, and has power-law tails $S(q) \propto q^{\eta-2}$ when $qL_{\text{eff}} \gg 1$. In the case of the Lorentzian line shape, if finite-size or instrumental resolution effects are to be included the Gaussian broadening must be numerically convoluted with the Lorentzian line shape.

The intrinsic line shapes must now be powder averaged because of the orientationally disordered nature of the *ZYX* substrate. In the case of the Lorentzian line shape this can be done analytically,

$$\int_0^{2\pi}\frac{d\varphi}{(\vec{Q}-\vec{\tau})^2+\kappa^2}=\frac{\pi}{Q\tau(d^2-1)^{1/2}}, \quad d\equiv\frac{\kappa^2+Q^2+\tau^2}{2Q\tau} , \tag{9}$$

where φ is the angle between $\vec{Q}$ and $\vec{\tau}$. This line shape is well approximated by the square root of a Lorentzian when $|\vec{Q}-\vec{\tau}| \ll \tau$ and $|\vec{Q}-\vec{\tau}| \gtrsim \kappa$. If we had used a Lorentzian instead of a powder-averaged Lorentzian, the peak halfwidths would have been equal to κ instead of $\sqrt{3}\kappa$. The powder-averaged form is almost certainly correct close to the freezing transition. A final convolution is necessary because of the vertical mosaic of the *ZYX* substrate. In the scattering cross section for a 2D crystal the Bragg spots are replaced by Bragg rods normal to the plane. If the crystal plane is tilted with respect to the scattering plane by an angle ψ, the scattering maximum will appear at a larger vector $\tau'=\tau/\cos(\psi)$. This leads to the well-known "sawtooth line shape" of 2D crystals.[80,81] Therefore, including an instrumental resolution and/or finite-size function $R(\vec{Q})$, the azimuthal powder average and the vertical mosaic average, an intrinsic line shape I_0 will be convoluted to give

$$I(Q)=\int d^3Q' R(\vec{Q}-\vec{Q}') \times\int d\vartheta\int d\psi P(\psi) I_0\left[|\vec{Q}'|-\frac{|\vec{\tau}|}{\cos\psi}\right]\cos\psi . \tag{10}$$

Here $\vec{\tau}$ is a reciprocal-lattice vector, ϑ is the angle of $\vec{\tau}$ relative to some arbitrary direction in the basal plane, and $P(\psi)$ is the probability that a crystalline plane is tilted an angle ψ from the scattering plane. As discussed above the Lorentzian line shape was analytically powder averaged, but the resolution and/or finite-size and vertical mosaic integrals were done numerically. To minimize calculational time, fits were also done in which the powder-averaged Lorentzians were not convoluted with the resolution function; it was found that the values of κ thus obtained agreed with the resolution-convoluted values when the peak halfwidth was more than 1.5 times the instrumental limit. The power-law line shape incorporates the finite-size convolution in the Kummer-function approximation, but the powder average and vertical mosaic integral were done numerically. The rotating-anode data were then multiplied by a polarization factor $[1+\cos^2(2\vartheta)]/2$.

In addition to the intrinsic scattering due to the adsorbed xenon, there was a diffuse scattering background due to scattering from substrate phonons, Compton scattering, etc. Typical peak-to-background intensity ratios were 6:1 in the solid phase for both sets of experiments. This background scattering was measured when

there was no xenon in the cell and fitted to a smooth polynomial $B(Q)$. With xenon in the cell, diffuse background scattering was partially absorbed. This effect was taken into account with an "absorption factor" $b(P,T)$, so that the final scattering cross section was of the form

$$I_{\text{calc}}(Q)=b(P,T)B(Q)+\left[\frac{1+\cos^2(2\vartheta)}{2}\right]I(Q)\ , \quad (11)$$

where $I(Q)$ is the intrinsic 2D scattering cross section [Eq. (10)] including all convolutions (the polarization factor was used only with the MIT data). Plotted diffraction curves in this paper have all had the background scattering subtracted. Accurate knowledge of the background absorption factor $b(P,T)$ was important because precise measurement of the intrinsic scattering in the peak wings depends sensitively on the amount of diffuse background scattering to be subtracted. In the MIT experiments, it was possible to calculate the absorption factor *ab initio*,

$$b=\exp[-\alpha(l_s\rho_s+l_v\rho_v)]\ , \quad (12)$$

where $\alpha=330\ \text{cm}^2/\text{g}$ is the mass absorption coefficient for Cu $K\alpha$ x rays passing through xenon, l_s and l_v are the lengths of the x-ray path through the Xe 2D solid and Xe 3D vapor regions of the sample cell, and ρ_s and ρ_v are the mass densities of the 2D xenon solid and 3D xenon vapor. Typical calculated values were $b=0.7-0.85$. In the SSRL experiments the absorption factor could not be calculated with sufficient accuracy due to the large volume of the sample cell. Therefore, $b(PT)$, was obtained from the least-squares fits based on combined criteria of physical plausibility and maximum goodness of fit: Statistically significant negative signal after background subtraction was not permitted in any scan, and b was fixed for a given run at the value that gave the smallest average χ^2 for the entire run. Values of b obtained in this way agreed well with approximate *ab initio* calculations. In addition, both the scattering amplitude and the absorption factor were renormalized by the observed attenuation of the graphite (002) peak; this canceled some of the effects of fluctuating incident x-ray flux.

In the fits to a Lorentzian cross section, the possible fitting parameters were the scattering amplitude A, peak position τ, width κ, vertical mosaic (tilt distribution HWHM) M, effective size L, and absorption factor b. However, the absorption factor was fixed as discussed above. The crystal size was fixed at 2000 Å or π/δ, the instrumental resolution, whichever was smaller. The vertical mosaic, which was determined by the line-shape asymmetry and was an intrinsic property of the substrate, was held fixed at the best average value for that run (typically 11° HWHM). When the central portion of the peak is resolution limited, κ is determined by the peak-to-wing intensity ratio, which is quite sensitive to the background absorption factor. The power-law line-shape fits were done similarly: b, M, and L were fixed at their calculated or best average positions, and the free fitting parameters were the scattering amplitude, peak position, and exponent η. Rather than being determined by the slope of the scattering in the wings, as one might naively expect, η also is primarily determined by the peak-to-wing intensity ratio. The uncertainties in the absorption, effective size, and vertical mosaic were incorporated in the error bars for A, τ, κ, and η.

VI. HIGH-RESOLUTION DATA

We now present our high-resolution diffraction results. Figures 3 and 4 show the Xe (1,0) diffraction peaks from the SSRL I run, which was a closed-cell run that crossed the liquid-solid phase boundary at a coverage of approximately 1.1 monolayers. The scattered intensity was generally integrated for either 4×10^4 or 10^5 monitor counts at each point; the average monitor-count rate was 10^5 counts/15 sec. In these and succeeding figures, the background scattering has been subtracted. The solid lines in Fig. 3 are fits to a power-law line shape, while the solid lines through the higher-temperature scans in Fig. 4 are fits to a Lorentzian line shape, as described in the preceding section.

At $T=120$ K there is a sharp primary diffraction peak centered at $\tau=1.639\ \text{Å}^{-1}$, with a small amount of scatter-

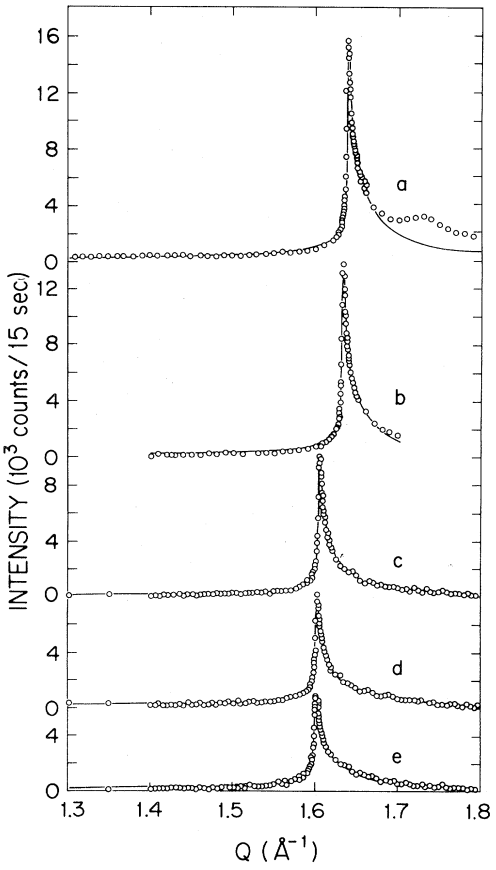

FIG. 3. SSRL I Xe(1,0) diffraction curves. Data points shown are characteristic; in some cases measurements were made on a finer mesh. Background has been subtracted. Solid lines are power-law fits. *a*, 120 K; *b*, 135 K; *c*, 150.0 K; *d*, 151.3 K; *e*, 151.6 K.

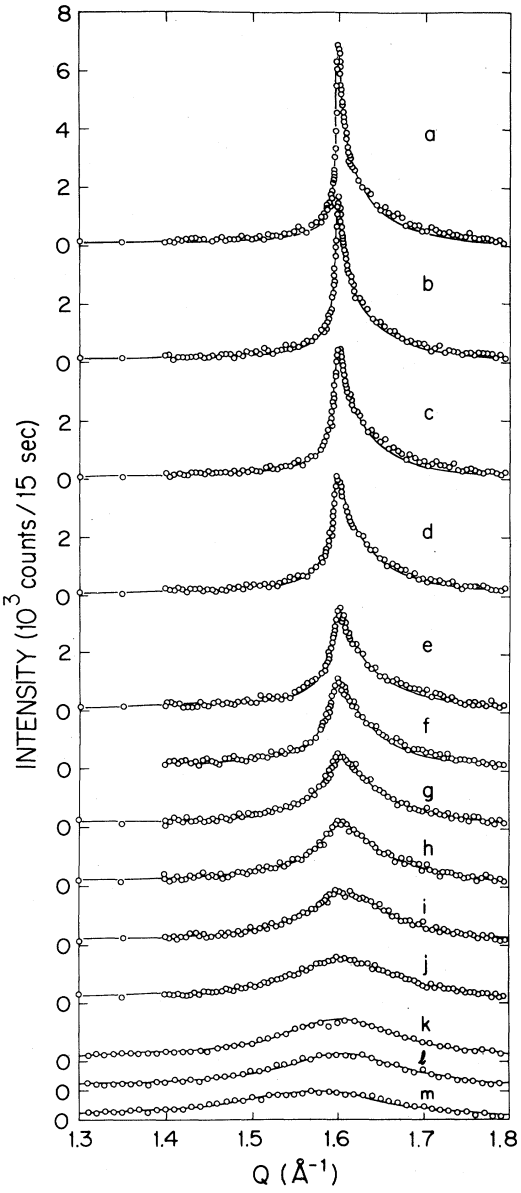

FIG. 4. SSRL I Xe(1,0) diffraction curves. Solid lines are Lorentzian fits. *a*, 151.60 K; *b*, 151.80 K; *c*, 151.90 K; *d*, 151.95 K; *e*, 152.00 K; *f*, 152.05 K; *g*, 152.10 K; *h*, 152.15 K; *i*, 152.25 K; *j*, 152.50 K; *k*, 153.0 K; *l*, 154.0 K; *m*, 160.0 K.

ing in the low-Q wing. There is also a broader, but well defined, peak at $Q \sim 1.73$ Å^{-1}. A calculation of the superstructure due to the hexagonal strain modulation predicts[82,83] a sharp superlattice peak at $\tau_{\text{comm}} + (\tau_{\text{comm}} - \tau_{\text{incom}})/2 \sim 1.73$ Å^{-1} if the adsorbed film is rotated 30° with respect to the substrate lattice vectors. The 120-K scan in Fig. 3 clearly shows that the modulation peak is much broader than the primary peak. This apparent discrepancy could be resolved if the orientation between the substrate and adsorbate were not perfectly rigid. Novaco and McTague[18] have shown that the energy of an adsorbed layer has a rather broad minimum as a function of orientational angle, which will be displaced from the high-symmetry direction. The observation of satellites around higher-order peaks would tend to confirm the description of a rotated monolayer; however, studies on oriented substrates are required to make an unambiguous determination of the orientation of the adsorbate. Between $T = 120$ and 150 K, the primary peak moves gradually to $\tau = 1.604$ Å^{-1} and remains sharp, the modulation peak becomes weaker and broader until it disappears, and the scattering in the wings increases slightly. Between $T = 150.0$ and 151.8 K, the peak broadens slightly, the scattering in the wings increases, and the reciprocal-lattice vector decreases to $\tau = 1.599$ Å^{-1}. Between $T = 151.80$ and 152.20 K, the correlations decrease dramatically. The central peak continuously becomes broader and weaker and the scattering in the wings increases. Since peak width is inversely proportional to positional correlation length, this means that the correlation length is decreasing. Scans above $T = 152.20$ K are clearly due to a fluid phase. The peak continues to broaden at a reduced rate, and the peak position moves to $\tau = 1.51$ Å^{-1} at $T = 178$ K. No evidence of hysteresis is seen.

All the diffraction peaks were first fitted to powder-averaged Lorentzian line shapes as described in the preceding section; it was found empirically that this line shape could describe both the solid and liquid line shapes satisfactorily. Table I shows the values of scattering amplitude, peak position, and κ from Lorentzian fits to the SSRL I run, as well as values of η from power-law fits to these scans. Fits below 150 K were done with a variable background parameter. Although the Lorentzian line shape is an incorrect description of the solid phase, it is a useful way to parametrize the shape of the diffraction curves. A background absorption factor of $b = 0.8$ gave the best fits above 150 K. Figure 5 shows the inverse correlation length κ obtained from Lorentzian fits to the SSRL I scans. Figure 6 shows the fitted peak position τ and peak amplitude A from Lorentzian fits, and the exponent η from power-law fits, to the SSRL I data. The error bars are estimated systematic errors due to uncertainty in the background absorption. Several features can be seen. The peak position evolves smoothly from $\tau \sim 1.605$ to 1.58 Å^{-1}, corresponding to a 1.5% lattice expansion. The fitted amplitude, which is proportional to the azimuthally averaged scattered intensity at the peak position, decreases smoothly and rapidly from 20 (arbitrary units) at $T = 151.6$ K to 0.4 at $T = 152.2$ K. The most dramatic curve is that describing the inverse correlation length κ versus temperature. At $T = 150$ K, the peak has a finite-size-limited width. Between $T = 151.6$ and 152.3 K, the inverse correlation length increases rapidly and continuously to $\kappa = 0.03$ Å^{-1}, corresponding to a correlation length of 30 Å, or about seven nearest-neighbor distances. At $T = 156$ K, $\kappa = 0.0554$ Å^{-1}, and at $T = 178$ K, $\kappa = 0.1$ Å^{-1}, corresponding to next-nearest-neighbor correlations only.

The solid lines in Fig. 5 are the results of a fit of κ vs T to the KTHNY prediction [Eq. (2)],

TABLE I. Fits to SSRL I diffraction scans.

T (K)	χ^{2a}	A^a	τ^a (Å^{-1})	κ^a (Å^{-1})	κ^b (Å^{-1})	χ^{2c}	η^c
120.0	59.0	36.6	1.638 84	0.000 43	0.000 17	40.0	0.23
125.0	8.4	34.5	1.635 73	0.000 55		7.0	0.26
130.0	5.6	33.2	1.631 29	0.000 54			
135.0	10.8	28.6	1.631 67	0.000 47	0.000 29	9.0	0.26
140.0	5.1	27.6	1.620 69	0.000 49		6.4	0.25
145.0	6.8	27.4	1.612 37	0.000 43		6.5	0.25
150.0	4.5	17.8	1.604 40	0.000 60	0.000 30	5.4	0.273
150.50	6.8	15.9	1.603 11	0.000 67	0.000 33	3.8	0.292
151.00	5.9	13.3	1.601 61	0.000 77	0.000 45	3.1	0.306
151.30	5.7	11.82	1.600 80	0.000 86	0.000 55	3.5	0.324
151.60	5.3	8.64	1.599 84	0.001 23	0.000 86	2.9	0.361
151.80	4.4	5.49	1.599 1	0.002 20	0.001 77	5.8	0.429
151.90	3.1	3.79	1.598 7	0.003 55	0.003 09	9.5	0.490
151.95	2.6	3.04	1.598 6	0.004 83	0.004 33	9.5	0.512
152.00	2.9	2.37	1.598 3	0.006 91	0.006 22		
152.05	2.1	1.87	1.597 6	0.009 7			
152.10	1.6	1.448	1.597 9	0.014 5			
152.15	1.3	1.164	1.597 8	0.020 4			
152.20	1.3	0.968	1.596 8	0.027 4			
152.25	0.9	0.967	1.596 6	0.026 9			
152.30	1.5	0.897	1.595 9	0.030 8			
152.40	1.4	0.854	1.596 1	0.032 6			
152.50	1.5	0.789	1.593 9	0.036 2			
152.70	1.7	0.763	1.592 3	0.037 3			
153.0	2.0	0.697	1.591 3	0.043 6			
154.0	1.6	0.630	1.588 7	0.046 6			
156.0	2.3	0.545	1.578 7	0.053 5			
160.0	2.0	0.455	1.56 5	0.06 2	0.072		
178.0	3.1	0.301	1.51 0	0.09 7			

[a]Results of fits to powder-averaged Lorentzians. A is proportional to the peak scattered intensity in this model.

[b]Results of fits to powder-averaged and resolution-convoluted Lorentzians.

[c]Results of fits to power-law line shapes.

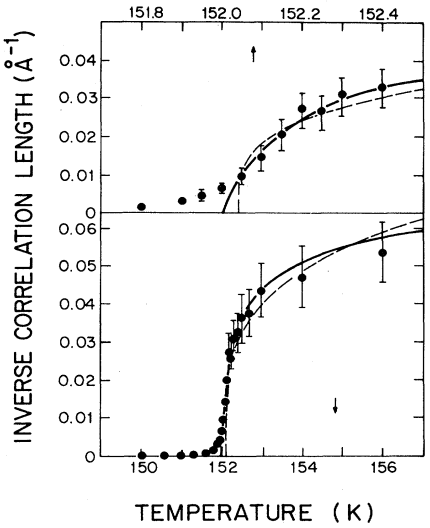

FIG. 5. Inverse correlation lengths from Lorentzian fits to SSRL I scans. Solid lines are fits to KTHNY form; dashed lines are power-law fits as discussed in text. Top and bottom panels are the same fits with different scales.

$$\kappa(T)=\kappa_0\exp\left[-B\left[\frac{T_c}{T-T_c}\right]^{\nu}\right], \tag{13}$$

with $\nu=0.4$ ($\nu=0.37$ gives an equally good result), $\kappa_0=0.082$ Å^{-1}, $B=0.0862$, and $T_c=152.00$ K. The fitted parameters depended sensitively on which points were included in the fit; the final values were 0.08 Å$^{-1}\leq\kappa_0\leq 0.18$ Å^{-1}, $0.08\leq B\leq 0.22$, and 151.80 K$\leq T_c\leq$152.00 K. It should be noted that the theoretical curve actually has a sigmoidal shape and approaches the temperature axis tangentially for temperatures extremely close to T_c. The exponential prediction lies within the error bars of the measured inverse correlation lengths except for the points at $151.8\leq T\leq 52.0$ K, where the calculated κ is too small. We will discuss the possibility that this effect is due to a first-order coexistence region in more detail below; the most likely explanation of the transition rounding is that finite-size and edge effects are playing a role. Quite possibly, binding-energy heterogeneity effects also round the transition to some extent.[84] At $T=151.90$ K, the correlation length is 325 Å. Since the limiting crystallite size is $L=2000$ Å, it is probable that when the correlation length reaches 300–500 Å edge effects begin

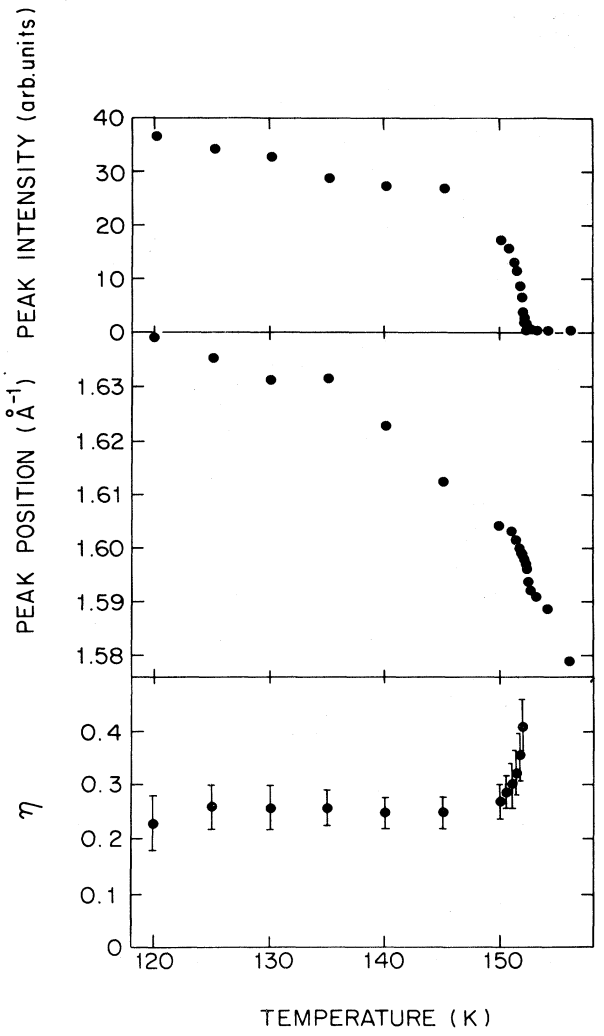

FIG. 6. Fitted parameters from SSRL I scans. Upper part is amplitude (Lorentizian line shape). Middle is peak position (Lorentzian line shape). Bottom part is η.

to play a role. Since the xenon nearest-neighbor distance is ~ 4.55 Å, a correlation length of 500 Å would imply correlated fluid patches containing roughly 10 000 atoms. Greif *et al.*[85] and Cardy[86] have calculated the width of the transition region in the KTHNY model; they argue that the KTHNY prediction [Eq. (13)] is only quantitatively exact when $\xi \gg 10^8$ lattice spacings. It is clear that our experiments do not probe this asymptotic region. Nevertheless, within our uncertainties the observed evolution of fluid correlation lengths is consistent with the KTHNY prediction with a fitted factor in the exponential.

The exponential form [Eq. (13)] for the inverse correlation length is unusual; for conventional phase transitions one observes a power-law evolution of the correlation length near the critical point. The dashed line in Fig. 5 is a fit to a power-law form,

$$\kappa = \kappa_0 \left[\frac{T - T_c}{T_c} \right]^{\nu}, \tag{14}$$

with $T_c = 152.04$ K, $\nu = 0.277$, and $\kappa_0 = 0.24$ Å^{-1}. The allowed ranges of the parameters are $151.85 \leq T_c \leq 152.05$, 0.24 Å$^{-1} \leq \kappa_0 \leq 0.9$ Å^{-1}, and $0.2 \leq \nu \leq 0.5$. A value $\nu \sim 0.3$ does not correspond to any known model and indeed in 2D systems one typically finds $\nu \sim 0.8-1.3$. The power-law form fits the data almost as well as the exponential form, and misses the same points at $T = 151.80$ and 151.90 K. The primary source of the error bars for κ_0 and ν is the uncertainty in T_c.

The diffraction peaks between $T = 120$ and 151.95 K were also fitted to a power-law line shape, as described in the preceding section. The results of these fits are summarized in Table I. The background was fixed at $b = 0.8$, with fluctuations renormalized by the intensity of the graphite (002) peak. This procedure worked well for $T > 150$ K. Between $T = 135$ and 120 K the integrated intensity under the Gr(002) peak decreased by 20%, while the integrated intensity in the wing of the xenon peak, between $Q = 1.30$ and $Q = 1.35$ Å^{-1}, decreased by 40%. The sudden decrease in transmission is probably due to a first-order second-layer condensation transition. When the second layer condenses the vapor pressure drops suddenly, and more of the gas is on the substrate and in the path of the x-ray beam. The second-layer condensation interpretation is strengthened by the observation that, while the reciprocal-lattice position changes continuously at higher temperatures due to thermal lattice expansion, the peak position remains nearly constant at $\tau = 1.615(2)$ Å^{-1} between $T = 130$ and 135 K. The discrepancy between the absorption of the Gr(002) peak and the xenon background signal is not understood; it is conceivably due to interference between the graphite planes and the adsorbed xenon layers. The solid line for the $T = 120$ K scan in Fig. 3 was generated by a least-squares fit in which $b(P,T)$ was allowed to vary. The fit shown gave $b = 0.219$ (i.e., 22% signal transmission); larger values resulted in negative subtracted counts on the wings. We emphasize, however, that the background was well behaved in the neighborhood of the melting transition.

Figure 6 shows the fitted values of η between $T = 120$ and 151.95 K. Error bars on η are estimated systematic errors due to uncertainties in background subtraction, crystallite size, and vertical mosaic. The error bars for η increase below $T = 150$ K. This is due to the anomalous background absorption described above, the high-Q modulation peak, and the more limited range of the scans. The exponent evolves slowly from $\eta = 0.25 \pm 0.07$ at $T = 125$ K to $\eta = 0.30 \pm 0.05$ at 150.5 K. Above $T = 151$ K, η increases rapidly to a value $\eta(T = 151.95\ \text{K}) = 0.512$. The quality-of-fit parameter increases rapidly from $\chi^2 = 2.9$ at $T = 151.6$ K to $\chi^2 = 9.5$ at $T = 151.95$ K. The power-law line shape cannot describe the high-temperature curves accurately because increasing η increases the value of the function in the wing, but leaves the width of the central part of the peak unchanged, while the measured scattering has an appreciably broadened central region. When

$T \geq 151.8$ K, the peaks must be described by a highly correlated fluid, possibly with edge effects playing a role. If we take the increase in χ^2 as an indication that the power-law line shape is no longer valid, then the largest believable value of the exponent is in the range $0.31 \leq \eta \leq 0.42$.

Scans in the solid-liquid transition region were also analyzed according to a simple model for a first-order phase transition. A closed-cell run will pass through a coexistence region, in which the solid material is converted into fluid according to a lever law. At a given (Θ, T) point in the coexistence region, the scattering function is given by

$$I(\vec{q},T,\Theta)=\alpha I_{\text{liq}}(\vec{q},T,\Theta_{\text{liq}})+(1-\alpha)I_{\text{solid}}(\vec{q},T,\Theta_{\text{solid}}) , \quad \alpha=\frac{\Theta-\Theta_{\text{solid}}}{\Theta_{\text{liq}}-\Theta_{\text{solid}}} , \tag{15}$$

where Θ_{liq} and Θ_{solid} are the coexistence-region boundaries at the temperature T and I_{liq} and I_{solid} are the scattering line shapes at those boundaries. We assume that the solid and fluid correlation lengths are relatively constant along the phase boundaries; the solid peak position at melting was found in the MIT experiments to be almost constant along the melting curve. Fits were done to the SSRL I scans assuming various coexistence boundaries. The diffraction line shape was generated by linear interpolation between best-fit line shapes at the assumed phase boundaries. χ^2 was then calculated for scans at temperatures between the coexistence boundary temperatures T_s and T_l with no adjustable parameters, assuming $\alpha=(T-T_s)/(T_l-T_s)$. Figure 7 shows the values of χ^2 from these fits with various assumed endpoints. The pure Lorentzian, single-phase fits give $2 \leq \chi^2 \leq 5$ (dashed line). $T=151.3$ K is clearly not the solid-phase boundary, since this choice

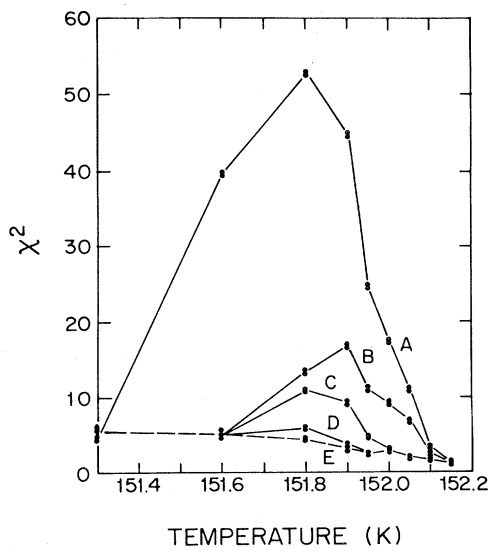

FIG. 7. Value of χ^2 from coexistence fits to SSRL I scans. Coexistence region boundaries are *A*, 151.3–152.15; *B*, 151.6–152.15; *C*, 151.6–152.05; *D*, 151.6–151.95; *E* single-phase Lorentzian fits (dashed line).

results in $\chi^2=53$ at $T=151.8$ K. Both the peak position and the overall shape are incorrect in this fit. As the coexistence-region boundaries are brought closer together, the fits predictably improve. When the coexistence limits are $T_s=151.6$ K, $T_l=151.95$ K, the single-phase and coexistence fits are essentially indistinguishable. Since the single Lorentzian inverse correlation length at $T=151.6$ K is $\kappa=0.001\,23$ Å$^{-1}=1/816$ Å, it is not physically plausible to assume that the solid coexistence-region boundary is at any higher temperature.

In another model for two-phase coexistence, a distribution of binding energies may result in an effective spread in transition temperatures.[84] Accordingly, we did a set of fits in which the amplitude of a sharp, solidlike peak and all of the parameters of an additional broad Lorentzian were allowed to vary. The width and position of the "solid" peak were fixed at their 151.6 K values. The values of κ thus obtained increased by 10–15%, but showed the same qualitative evolution up to $\xi=250$ Å. We therefore conclude that the xenon melting transition at $T \sim 152$ K, as measured in a closed-cell run, shows a continuous evolution of the correlation length up to at least 200 Å, and is consistent with a continuous transition at longer length scales, but that two-phase coexistence over the very narrow temperature range between $T=151.6$ and 151.95 K cannot be ruled out. Note that the melting transition, although apparently continuous, is quite rapid; κ evolves from the reciprocal of the finite-size limit to half of its liquid saturation value between $T=151.8$ and 152.3, 0.003 in reduced temperature.

A second run, SSRL II, was done as a function of vapor pressure at a constant temperature $T=150.0$ K. Such an experiment differs qualitatively from a closed-cell run. Because the 3D vapor pressure is proportional to exp(chemical potential), and phases in equilibrium must have the same chemical potential, a first-order transition will manifest itself as a discontinuous change in the scattering profiles as a function of pressure; that is, a discontinuous jump in the fitted correlation length as a function of pressure is the signature of a first-order transition, while a continuous evolution of the correlation length indicates a continuous transition. However, even a first-order transition may show some rounding due to macroscopic disorder, resulting in apparent two-phase coexistence. The diffraction peaks from this run are shown in Fig. 8; they are closely similar to those in the SSRL I run. No evidence of hysteresis is seen. At $P=40.0$ Torr the diffraction line shape is a finite-size-limited central peak with extended wings, centered at $\tau=1.600$ Å^{-1}. With decreasing pressure, the peak continuously becomes broader and weaker. At $P=31.0$ Torr, the peak is quite broad, weaker by a factor of 6, and centered at $\tau=1.59$ Å^{-1}.

The least-squares fits were done in the same way as for the SSRL I peaks. Owing to problems with the electron-storage-ring stability, the x-ray intensity fluctuated considerably, and this problem was not completely eliminated by the practice of dividing by the monitor signal and normalizing to the Gr(002) integrated intensity. Therefore, both the data and fits in this run are of slightly lower

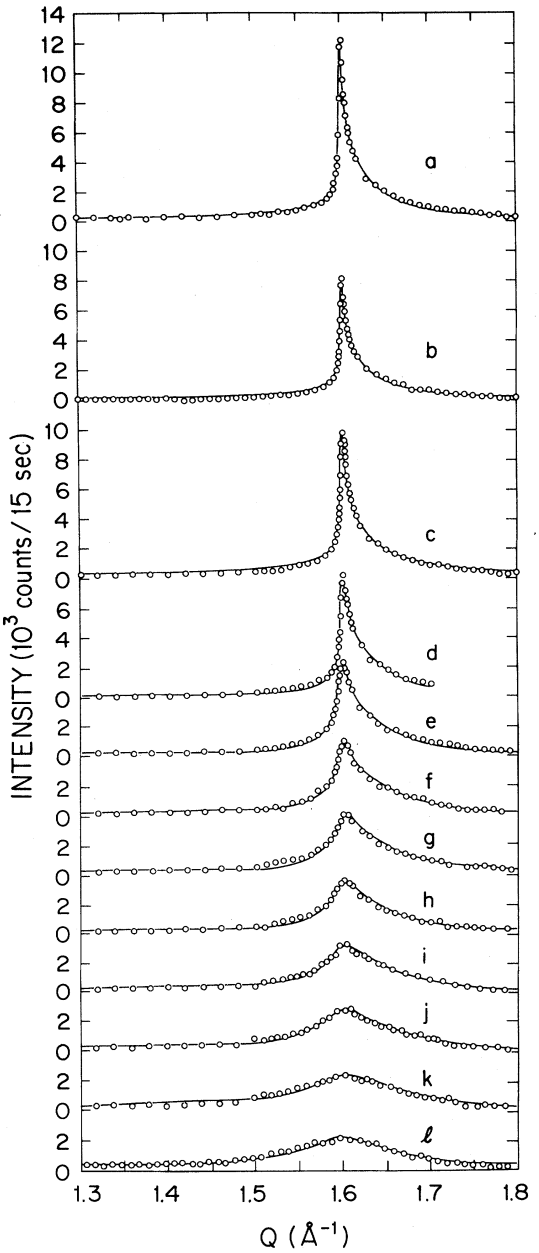

FIG. 8. SSRL II Xe(1,0) diffraction curves as a function of pressure (in Torr) at $T=150$ K: *a*, 40.0; *b*, 38.19; *c*, 37.0; *d*, 35.9; *e*, 35.43; *f*, 35.05; *g*, 34.7; *h*, 34.50; *i*, 34.35; *j*, 34.00; *k*, 33.0; *l*, 31.0. Solid lines for $P \geq 37.0$ Torr are power-law line shapes; the rest are Lorentzians.

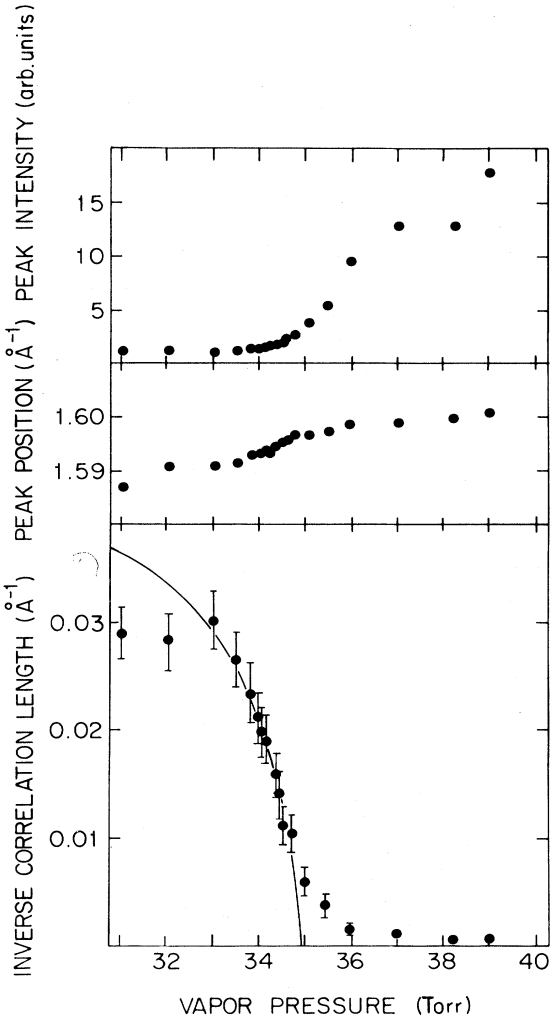

FIG. 9. Peak amplitude, peak position, and inverse correlation lengths from Lorentzian fits to SSRL II scans. Solid line is a functional form $\kappa=\kappa_0\exp\{-B[P_c/(P_c-P)]^\nu\}$ with empirically chosen parameters $\kappa_0=0.082$ Å^{-1}, $P_c=35$ Torr, and $B=0.33$.

quality than those in SSRL I. In particular, the most fluid peaks (large κ) have large error bars in κ due to the uncertainty in the subtracted background. This, combined with the lack of diffraction data well into the fluid phase, precluded detailed fits of κ vs P, since the saturation value κ_0 was undetermined. Fitted values of κ, peak position, and amplitude from Lorentzian fits to the SSRL II scans are shown in Fig. 9. The inverse correlation length evolves continuously from $\kappa=0.0006$ Å^{-1} at $P=40.0$ Torr to $\kappa=0.029$ Å^{-1} at $P=31.0$ Torr without any observable discontinuity. The solid line in Fig. 9 is a functional form

$$\kappa=\kappa_0\exp\{-B[P_c/(P_c-P)]^\nu\}$$

with empirically chosen parameters $P_c=35$ Torr, $B=0.33$, and $\kappa_0=0.082$ Å^{-1} (i.e., κ_0 was fixed at its saturation value from the SSRL I scans). Consistent with the results described for the SSRL I data, there is some rounding of the transition below $\kappa=0.004$ Å$^{-1}\sim 1/250$ Å. In this case, however, a substantial variation in substrate binding energies would be required to explain the rounding. The scans at pressures above 35.43 Torr were fitted to power-law line shapes. The measured exponents were η (40 Torr)$=0.311$, η(38.19 Torr)$=0.323$, η(37.0 Torr)$=0.374$, and η(35.9 Torr)$=0.420$. The power-law fit to the 35.9-Torr scan resulted in $\chi^2=10.0$, as opposed

to $\chi^2=5.6$ for a Lorentzian fit. We conclude that for this run, $\eta(\text{melting})=0.37\pm0.05$. As with the closed-cell measurements, "coexistence" fits were done with a Lorentzian plus a sharp peak (with width and position fixed by the fit at 37.0 Torr) with arbitrary amplitude to mimic the effects of a spread in T_c. Again, the fitted values of κ increased slightly, but the observed evolution in correlation length remained continuous.

As discussed in Sec. II the KTHNY theory makes a prediction [Eq. (4)] for the peak scattering on the liquid side of the transition as a function of correlation length. For all models discussed quantitatively to date, the liquid structure has been given by a single-pole Lorentzian. So we write

$$I(\vec{Q})=\frac{A\kappa^{\eta}}{\kappa^2+(\vec{Q}-\vec{\tau})^2}\ , \tag{16}$$

$$I(\vec{\tau})\propto\kappa^{\eta-2}\ . \tag{17}$$

Since Xe on ZYX is a powder in the plane, the measured scattering function is an integral of the intrinsic scattering around a circle of radius τ,

$$I'(\tau)\propto\int_0^{2\pi}d\vec{Q}\,'I(\vec{Q}\,')R(\vec{\tau}-\vec{Q}\,')\propto\kappa I(\vec{\tau})\ ,$$
$$I_{\text{measured}}(\tau)\propto\kappa^{\eta-1}\ . \tag{18}$$

The amplitude parameter A in the Lorentzian fits is proportional to the measured peak intensity. Figure 10 shows the fitted values of A from the Lorentzian fits to the SSRL I and SSRL II scans, rescaled to fall on the same curve. The function $A=A_0\kappa^{-0.72}$ fits the data well, implying that $\eta=0.28\pm0.05$. This is in good agreement with the measured value of η on the solid side of the transition and the prediction [Eq. (4)]. The power-law evolution of A vs κ should occur when $[(T-T_c)/T_c]\ll1$; the success of the prediction when $\kappa=0.04$ Å$^{-1}=1/25$ Å, quite far from the transition, is possibly fortuitous.

The last high-resolution run, SSRL III, was done as a function of surface coverage near $\Theta=0.85$ at $T=112$ K, where the melting transition is known from isotherm measurements and previous scattering measurements to be first order.[66] Figure 11 shows the Xe(1,0) diffraction peaks at surface coverages $\Theta=0.897$, 0.855, 0.837, 0.829, 0.812, and 0.767 monolayers. Possibly because of additional x-ray absorption or Compton scattering by the adsorbed xenon, the background normalization procedure previously described was unsuccessful, and a small term linear in Q was added to the intrinsic Lorentzian line shape. The solid lines in Fig. 11 are fits to a Lorentzian line shape. This function describes the scans at $\Theta=0.897$, 0.829, 0.812, and 0.767 well. However, even with various corrections to the background the scans at $\Theta=0.855$ and 0.837 could not be described by a single Lorentzian line shape, which was too weak in the wings and not sharp enough in the center to describe the measured peaks. Figure 12 shows fits to a two-Lorentzian composite line shape at $\Theta=0.855$ and 0.837. Owing to the limited number of experimental points, the coexistence line shapes could not be determined *a priori,* but it was required that the two scans be sums of a sharp and a broad line shapes with all parameters except amplitudes equal for the two fits, and that the solid line shape has a physically plausible $\kappa\leq0.00125$ Å^{-1}. The fitted curves in Fig. 12 have $\tau_l=1.575$ Å^{-1}, $\kappa_l=0.0335$ Å^{-1}, $\tau_s=1.582$ Å^{-1}, and $\kappa_s=0.00125$ Å^{-1}. The two-Lorentzian line shapes work

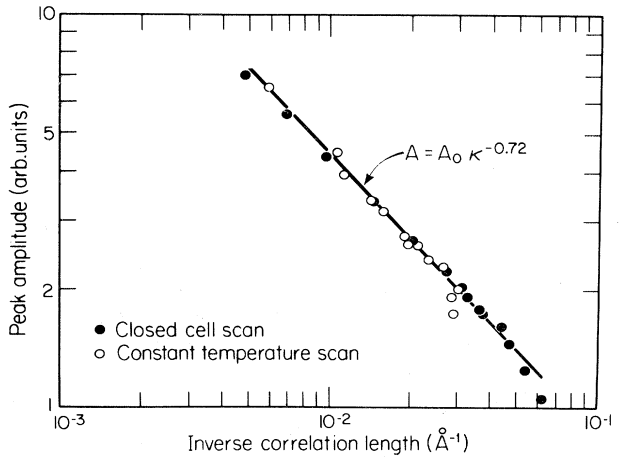

FIG. 10. Fitted amplitudes from SSRL I and SSRL II runs vs fitted κ. Amplitudes are proportional to peak intensity and are normalized to lie on the same curve.

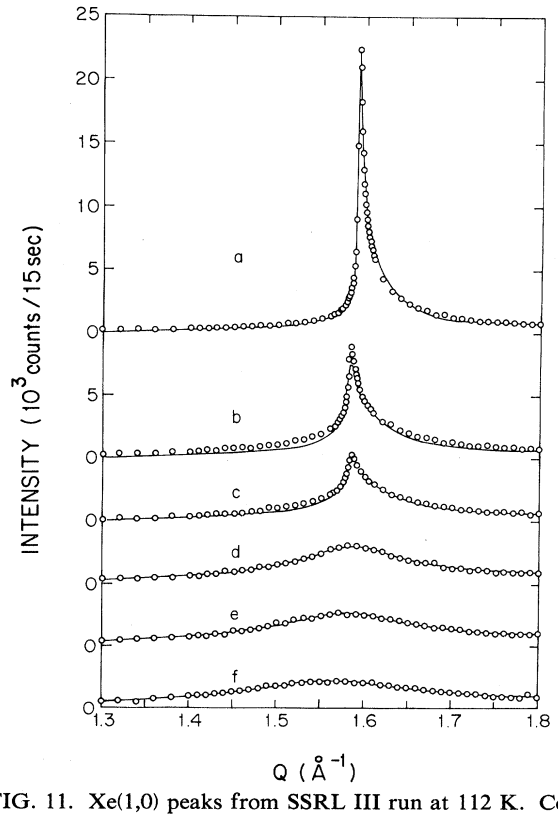

FIG. 11. Xe(1,0) peaks from SSRL III run at 112 K. Coverages (in units of 1 monolayer) are *a*, 0.897; *b*, 0.855; *c*, 0.837; *d*, 0.829; *e*, 0.812; *f*, 0.767. Solid lines are fits to a single Lorentzian plus a small linear term.

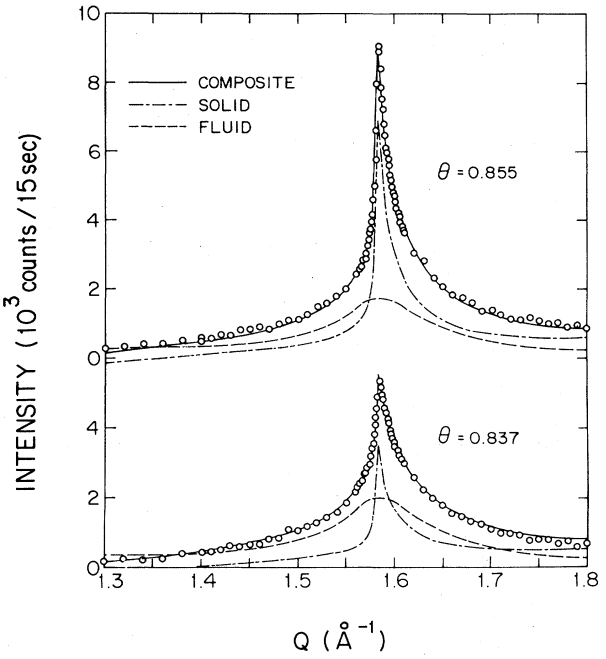

FIG. 12. SSRL III scans at $\Theta=0.855$ and 0.837. Solid line is a fit to a composite line shape; other two lines are constituent liquid and solid line shapes.

well, but χ^2 is relatively insensitive to the exact values of the parameters used. Extrapolating the values of τ and κ from their fitted values in the pure solid and liquid phase, we deduce boundaries $\Theta=0.833$ and 0.867 which agree quite well with the Thomy and Duval[57] values $0.84\leq\Theta$ (two phase) ≤ 0.88, and the limits measured by Hammonds[66] $0.83\leq\Theta$ (two phase) ≤ 0.90. We conclude, therefore, that two-phase coexistence has a subtle but distinct signature in the measured scattering line shape when high-resolution scans are performed, which was not observed in the high-coverage melting transition experiments. The locations of the phase boundaries as determined by diffraction line-shape analysis are in excellent agreement with the locations determined by other workers using thermodynamic measurements.

VII. LOW-RESOLUTION DATA

As discussed earlier the MIT experiments were performed in advance of the synchrotron measurements. These experiments employed a rotating-anode x-ray generator with a graphite monochromator. The diffraction runs were done in the closed-cell mode at doses corresponding to zero-temperature coverages of 1.01, 1.26, 1.33, 1.57, 1.59, and 1.84 monolayers. The approximate paths traced through the phase diagram in these runs are shown in Fig. 2. The instrumental resolution was $\Delta q=0.0085$ Å^{-1} HWHM, which is equivalent to scattering from finite platelets with $L_{\rm eff}=370$ Å. All the diffraction lines were analyzed with Lorentzian line shapes. As discussed in the section on data analysis, when $\xi\ll L_{\rm eff}$, the fitted value of κ is determined by the diffraction peak halfwidth, but, when $\xi\gg L_{\rm eff}$, κ is determined by the peak-to-wing intensity ratio. Some of the peaks were also analyzed with a power-law line shape, again with $L_{\rm eff}=370$ Å. The MIT1.59 run was the most thorough and was representative of the other runs, so we will discuss it in detail.

Figure 13 shows selected Xe(1,0) diffraction peaks from the MIT1.59 run. The average monitor signal rate was (5×10^4 counts/sec), and the scattered intensity was integrated for at least 1.5×10^6 monitor counts at each point. Solid lines are fits to power-law line shapes for $T\leq 152.7$ K and Lorentzian line shapes for $T\geq 152.9$ K. The line-shape evolution is qualitatively the same as that in the SSRL I scans. At $T=80.1$ K the scattering consists of a resolution-limited peak centered at $\tau=1.6618$ Å^{-1} and a modulation peak at $Q\sim 1.73$ Å^{-1}. The primary peak can be described either as a power-law singularity with $\eta=0.21\pm.05$ or a Lorentzian with $\kappa=0.0005\pm0.000\,33$ Å^{-1}. Unfortunately, there was a broad peak in the empty-cell background centered at $Q=1.7$ Å^{-1}, presumably due to adsorbed impurities, which varied somewhat with time and temperature. Although this impurity peak could be included in the sub-

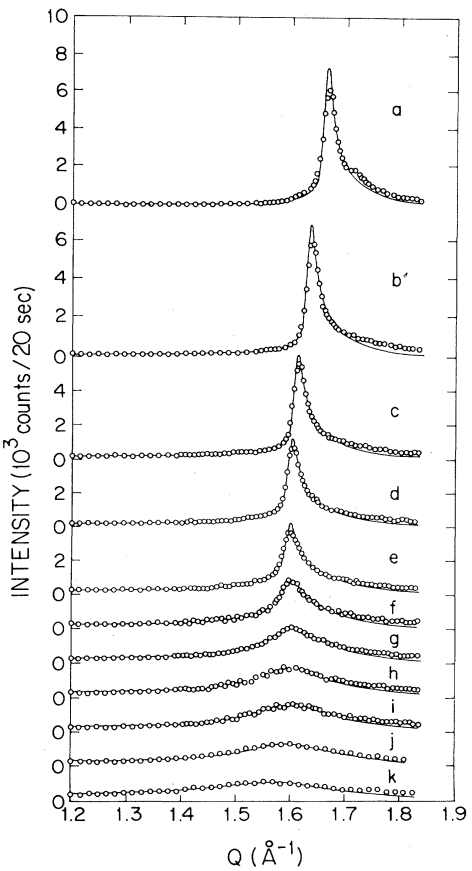

FIG. 13. MIT1.59 Xe(1,0) diffraction curves: *a*, 80.1 K; *b*, 124.7 K; *c*, 146.0 K; *d*, 151.5 K; *e*, 152.7 K; *f*, 152.9 K; *g*, 153.2 K; *h*, 153.5 K; *i*, 154.0 K; *j*, 157.6 K; *k*, 171.4 K. For $T\leq 152.7$ K, solid lines are power-law fits; the rest are powder-averaged, resolution-convoluted Lorentzian fits as discussed in the text.

tracted background function, and thus eliminated to first order, a careful determination of the Xe modulation peak at 1.73 Å^{-1} was not possible in this experiment. As the temperature increases, the lattice expands, the scattering in the wings increases, and the modulation peak becomes broader and weaker. At $T=152.67$ the peak may be described as a power-law singularity with $\eta=0.36\pm0.05$ or a Lorentzian with $\kappa=0.0043$ Å^{-1}. The peak at $T=152.67$ is describable either with $\eta=0.46\pm0.10$ or with $\kappa=0.0106$ Å$=1/94$ Å. By the time the correlations have diminished to 94 Å, the SSRL scans are unambiguously described as Lorentzians due to well-correlated fluids. The transition temperature and critical properties of the melting transition are less well determined in the low-resolution scans due to difficulty in distinguishing experimentally the correct line shape. The MIT1.59 fits yield $0.25\leq\eta(\text{melting})\leq0.45$. Fitted values of η are listed in Table II.

TABLE II. Fits to MIT1.59 Xe(1,0) diffraction peaks.

T (K)	A[a]	τ[a] (Å^{-1})	κ[a] (Å^{-1})	η[b]
80.1	4.17	1.6618	0.000 64	0.208
90.5	3.80	1.6541	0.000 41	0.195
99.3	3.71	1.6488	0.000 41	0.196
106.4	3.59	1.6444	0.000 37	0.193
110.9	3.95	1.6421	0.000 55	0.209
115.5	3.89	1.6393	0.000 56	0.211
120.1	4.06	1.6369	0.000 74	0.224
124.7	4.16	1.6338	0.000 87	0.234
129.0	4.42	1.6307	0.001 13	0.251
133.7	4.36	1.6265	0.001 25	0.257
134.1	4.26	1.6262	0.001 26	0.255
138.8	4.19	1.6214	0.001 49	0.266
142.2	4.15	1.6169	0.001 76	0.279
144.1	4.20	1.6141	0.002 00	0.288
146.0	4.22	1.6113	0.002 24	0.298
148.0	4.44	1.6080	0.002 81	0.299
149.2	4.64	1.6061	0.003 4	0.334
150.5	4.80	1.6034	0.004 3	0.360
151.0	4.86	1.6024	0.004 3	0.358
151.5	4.80	1.6014	0.004 7	0.366
151.7	4.95	1.6009	0.005 1	0.374
151.9	5.03	1.6003	0.005 6	0.385
152.2	5.13	1.5999	0.006 2	0.395
152.4	5.49	1.5994	0.007 5	0.417
152.7	5.96	1.5989	0.010 6	0.459
152.9	6.27	1.5986	0.019 2	
153.1	7.68	1.5979	0.024 8	
153.2	8.32	1.5981	0.031 8	
153.3	8.69	1.597	0.035	
153.5	9.29	1.596	0.042	
153.8	9.52	1.596	0.046	
154.0	9.52	1.594	0.047	
154.4	9.56	1.593	0.049	
154.9	9.72	1.593	0.052	
155.4	9.74	1.592	0.055	
156.1	9.90	1.589	0.056	
156.7	8.75	1.585	0.052	
157.6	8.86	1.585	0.054	
158.6	9.03	1.584	0.057	
159.5	9.24	1.580	0.061	
161.4	9.18	1.575	0.062	
163.8	9.79	1.576	0.071	
165.7	9.41	1.571	0.071	
167.6	9.96	1.568	0.076	
169.5	10.3	1.570	0.082	
171.4	10.17	1.562	0.082	

[a]Results of fits to a resolution-convoluted, powder-averaged Lorentzian line shape. Peak scattered intensity is proportional to A/κ in this model.

[b]Results of fits to a power-law line shape.

Fitted values of κ from the MIT1.59 run using a resolution-convoluted, power-averaged Lorentzian line shape are summarized in Table II and plotted in Fig. 14. Fitted values of κ from the SSRL I run are also plotted with the temperature scale shifted $+0.8°$ so that the curves overlap in the fluid phase. The curves agree well in the fluid phase, but differ substantially at lower temperatures. Since the two scans were done under very similar conditions, we expect that the structure and correlations of the 2D crystallites should be the same; it appears that the fitted value of the inverse correlation length κ depends on the resolution. On the other hand, the value of η obtained from power-law fits does not move outside the error bars when the resolution is changed from 370 to 2000 Å. Lorentzian and power-law line shapes are qualitatively different in that the former has an intrinsic length scale $1/\kappa$ while the latter does not. Since changing the instrumental resolution corresponds to changing the length scale of the measurement, we expect that Lorentzian and power-law line shapes should scale differently.[78,87] The observed invariance of the fitted value of η under a length

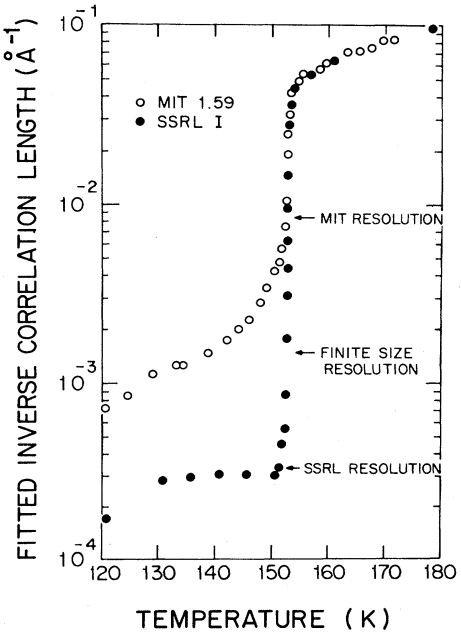

FIG. 14. Inverse correlation length vs temperature from SSRL I and MIT1.59 runs. The SSRL I temperature scale has been shifted by $+0.8$ K so that the curves superimpose when κ is large.

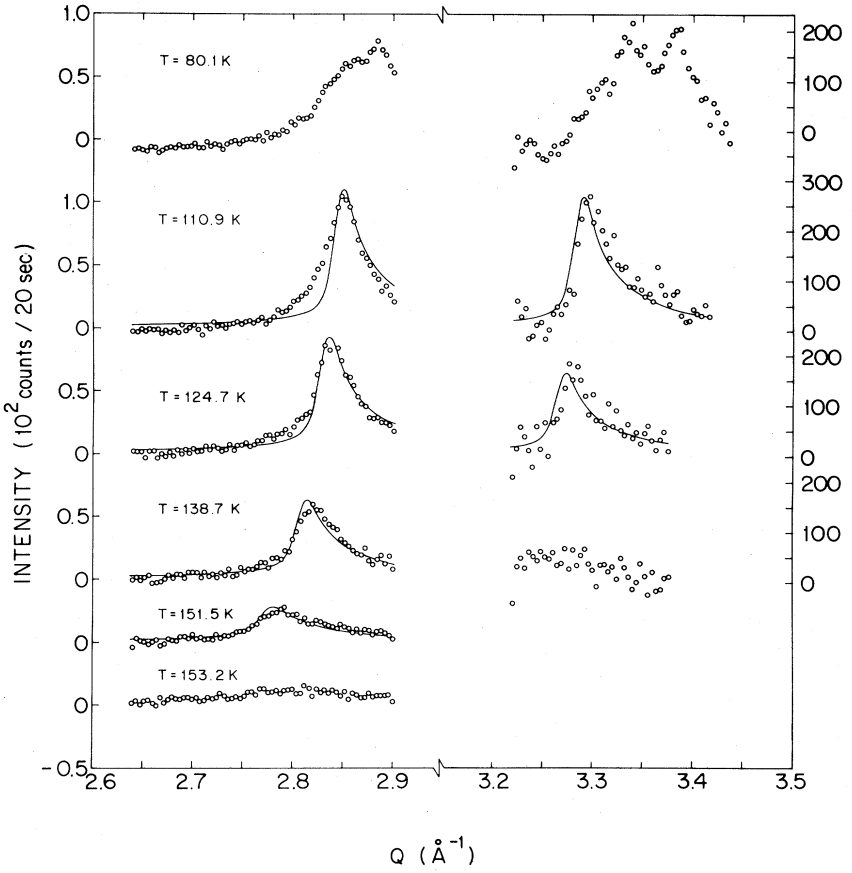

FIG. 15. MIT1.59 (1,1) and (2,0) peaks. Solid lines are Lorentzian fits with fixed τ and κ.

scale change is a strong indication that the power-law line shape contains a correct description of the physics.

Figure 15 shows higher-order peaks from the MIT1.59 run. At low temperatures substrate modulation peaks are visible. Because of the low signal-to-background intensity ratio, detailed investigation of the correlation function was precluded. The solid lines shown are Lorentzian fits with peak positions and halfwidths fixed from their fitted values in the equivalent Xe(1,0) peaks. Power-law fits were also done, and yielded $\eta(1,1)=0.5\pm0.25$ and $\eta(2,0)=0.7\pm0.3$ when $100\leq T\leq 130$ K. This is consistent with the more accurately measured $\eta(1,0)=0.25\pm0.05$ and the prediction $\eta\propto|\tau|^2$. In the future, we expect that careful measurements of the higher-order peaks will provide a sensitive test of the power-law line shape.

Diffraction scans from the other MIT runs are qualitatively similar to those in the MIT1.59 run. The trends found previously are seen in these runs: sharp peaks at low temperatures, lattice expansion and increased scattering in the wings with increasing temperature, and an apparently continuous melting transition. Plots of inverse correlation length versus temperature are also qualitatively similar. If we take as a rough criterion for the melting temperature $\kappa=0.005$ Å^{-1}, then as seen in Table III peak position at melting is given by $\tau_m=1.600\pm0.02$ Å^{-1} over the temperature range $112<T_m<152$ K. This justifies the assumption in the preceding section of constant lattice parameters along a hypothesized coexistence curve. The κ-vs-T curves all resemble one another and the curves measured in the high-resolution experiments. The fitted values of η at the melting transition are also consistent with that measured in the MIT1.59 run. Figure 16 shows fitted values of the normalized peak scattering intensity from all the MIT closed-cell runs versus inverse correlation length. Amplitudes have been corrected for background absorption and renormalized so that $A(\kappa=0.03$ Å$^{-1})\equiv 2$. Only values of κ above the resolution limit 0.005 Å^{-1} are plotted. The data are all consistent with a power law (peak intensity) $\propto\kappa^{-0.72}$ found in the SSRL data.

TABLE III. Melting parameters.

Run	Coverage	T_m	τ (Å^{-1})	η
SSRL I	1.10	152	1.598	0.36(08)
SSRL II	1.10	150	1.597	0.37(05)
SSRL III	0.85	112	1.58	
MIT1.01	0.90	138	1.599	0.32(10)
MIT1.26	1.00	146	1.600	
MIT1.33	1.02	148	1.603	
MIT1.57	1.10	149	1.607	
MIT1.59	1.10	151.7	1.601	0.35(10)
MIT1.84	1.20	150.0(2)	1.610	0.35(10)

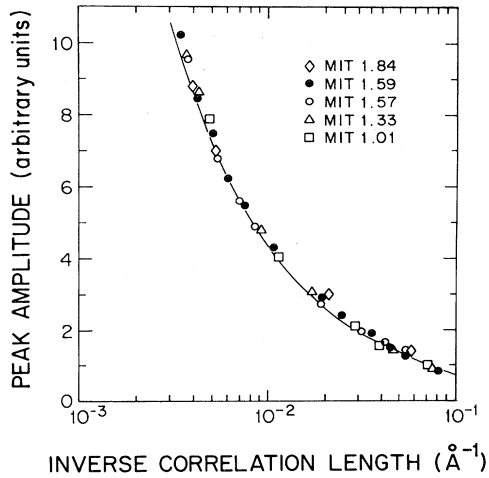

FIG. 16. Fitted peak intensities from MTT closed-cell data normalized to $A(\kappa=0.03)=2$. Solid line is a theoretical prediction $A \propto \kappa^{\eta-1}$ with $\eta=0.28$.

VIII. SUMMARY

At $T=150$ K and $\Theta=1.1$ our high-resolution x-ray scattering results indicate that the 2D xenon freezing transition is continuous. A power-law line shape describes the data well with a value of the correlation exponent in the solid phase,

$$0.27 \leq \eta(\text{melting}) \leq 0.42 , \tag{19}$$

consistent with the KTHNY prediction $0.25 \leq \eta(\text{melting}) \leq 0.33$. On the fluid side of the transition the evolution of the correlation length with temperature is consistent with the Halperin-Nelson-Young prediction of an exponential dependence of $\kappa(T)$, although we cannot preclude a power-law dependence with an anomalously small exponent ν. The correlation length evolves continuously to at least 200 Å before finite-size or edge effects affect the line shape. A narrow, substrate-induced coexistence region may occur when the correlation length exceeds 500 Å. The exponent η, measured by the evolution of peak intensity versus peak halfwidth on the fluid side of the transition, is found to be

$$0.23 \leq \eta \leq 0.33 . \tag{20}$$

Diffraction scans taken as a function of pressure at constant temperature also display these features with $\eta(\text{melting})=0.37\pm0.05$. The anomalous beam absorption observed below 135 K is consistent with a second-layer condensation transition. At 112 K the melting transition is deduced from line-shape analysis to be first order, consistent with the results of vapor-pressure isotherm measurements, and with the extrapolated multicritical point at $T \sim 125$ K.

The MIT low-resolution results are consistent in all respects with the high-resolution results. In particular, we find $\eta(\text{melting})=0.35\pm0.10$ both from line-shape analysis and from the evolution of peak intensity with peak width. In the solid phase, the change in the fitted correlation lengths under a change of resolution, as contrasted with the agreement of power-law exponents, offers strong support for the correctness of the power-law line shape; concomitantly the power-law correlations due to divergent long-wavelength phonons almost certainly provide the correct description of a continuous-symmetry 2D solid.

ACKNOWLEDGMENTS

We wish to acknowledge helpful discussions with B. I. Halperin, D. R. Nelson, S. K. Sinha, J. L. Cardy, and M. Sutton. We should also like to thank the SSRL staff for their generous assistance. This work was supported in part by the U.S. Joint Services Electronics Program under Contract No. DAAG-29-80-C-D104, by the U.S. Army Research Office under Contract No. DAAG-29-81-K-0029, and by the National Science Foundation through the Division of Materials Research.

*Present address: Department of Physics and Laboratory for Research on the Structure of Matter, University of Pennsylvania, Philadelphia, PA 19104.

†Present address: Department of Physics, State University of New York, Stony Brook, NY 11794.

‡Present address: Physics Department, Brookhaven National Laboratories, Upton, NY 11973.

[1] *Ordering in Two Dimensions,* edited by S. K. Sinha (Elsevier North-Holland, New York, 1980).

[2] J. G. Dash, *Films on Solid Surfaces; the Physics and Chemistry of Physical Adsorption* (Academic, New York, 1975).

[3] J. G. Dash and J. Ruvalds, *Phase Transitions in Surface Films* (Plenum, New York, 1980).

[4] *Ordering in Strongly Fluctuating Condensed Matter Systems,* edited by T. Riste (Plenum, New York, 1980).

[5] R. J. Birgeneau, P. A. Heiney and J. P. Pelz, Physica 109&110B, 1785 (1982).

[6] R. Peierls, Helv. Phys. Acta 7, Suppl.II, 81 (1934); R. Peierls, Ann. Inst. Henri Poincaré 5, 177 (1935).

[7] F. Bloch, Z. Phys. 61, 206 (1930).

[8] L. D. Landau, in *Collected Papers of L. D. Landau,* edited by D. Ter Haar (Gordon and Breach, New York, 1965), p. 209; L. D. Landau and E. M. Lifshitz, *Statistical Physics* (Pergamon, New York, 1958).

[9] N. D. Mermin and H. Wagner, Phys. Rev. Lett. 17, 1133 (1966); N. D. Mermin, J. Math. Phys. 8, 1061 (1976); N. D. Mermin, Phys. Rev. 176, 250 (1968); Phys. Rev. B 20, 4762(E) (1979).

[10] P. C. Hohenberg, Phys. Rev. 158, 383 (1967).

[11] D. Jasnow and M. E. Fisher, Phys. Rev. Lett. 23, 286 (1969); D. Jasnow and M. E. Fisher, Phys. Rev. B 3, 895 (1971); 3, 907 (1971).

[12] H. Mikesa and H. Schmidt, J. Low. Temp. Phys. 2, 371 (1970).

[13] B. Jancovici, Phys. Rev. Lett. 19, 20 (1967).

[14] Y. Imry and L. Gunther, Phys. Lett. 29A, 483 (1969); Y.

Imry and L. Gunther, Phys. Rev. B 3, 3939 (1971).
[15]B. Gavish and Y. Imry, J. Chem. Phys. 65, 139 (1976); Y. Imry, C. R. C. Crit. Rev. Solid State Mater. Sci. 8, 157 (1978).
[16]V. L. Berezinskii, Zh. Eksp. Teor. Fiz. 59, 907 (1970); [Sov. Phys.—JETP 32, 493 (1971)]; V. L. Berezinskii, *ibid.* 61, 1144 (1971) [*ibid.* 34, 610 (1972)].
[17]J. M. Kosterlitz and D. J. Thouless, J. Phys. C 5, L124 (1972); 6, 1181 (1973); 1, 1046 (1974); *Progress in Low Temperature Physics,* edited by D. F. Brewer (North-Holland, New York, 1978), Vol. VII B, Chap. 5.
[18]A. D. Novaco and J. P. McTague, Phys. Rev. Lett. 38, 1286 (1977); J. P. McTague and A. D. Novaco, Phys. Rev. B 19, 5299 (1979).
[19]B. I. Halperin and D. R. Nelson, Phys. Rev. Lett. 41, 121 (1978); 41, 519(E) (1978); D. R. Nelson and B. I. Halperin, Phys. Rev. B 18, 2318 (1978); 19, 2457 (1979).
[20]A. P. Young, Phys. Rev. B 19, 1855 (1979).
[21]D. S. Fisher, B. I. Halperin, and R. Morf, Phys. Rev. B 20, 4692 (1979).
[22]S. T. Chui, Phys. Rev. Lett. 49, 933 (1982).
[23]J. Z. Zittarz, Z. Phys. B 23, 55,63 (1976); J. Z. Zittarz and B. A. Huberman, Solid State Commun. 18, 1373 (1976).
[24]A. Luther and D. J. Scalapino, Phys. Rev. B 16, 1153 (1977).
[25]A. Holz and J. T. N. Mederios, Phys. Rev. B 17, 1161 (1978); A. Holz, in *Ordering in Two Dimensions,* Ref. 1, p. 313.
[26]P. Bak and D. Mukamel, Phys. Rev. B 19, 1604 (1979).
[27]T. V. Ramakrishnan and M. Yussouf, Phys. Rev. B 19, 2275 (1979); T. V. Ramakrishnan, Phys. Rev. Lett. 48, 541 (1982).
[28]B. J. Adler and T. E. Wainright, Phys. Rev. 127, 359 (1962).
[29]J. Q. Broughton, G. H. Gilmer, and J. D. Weeks, Phys. Rev. B 25, 4651 (1982), and references therein.
[30]F. F. Abraham, Phys. Rev. Lett. 44, 463 (1980); F. F. Abraham, Phys. Rep. 80, 339 (1981).
[31]F. Koch and F. F. Abraham, Phys. Rev. B 27, 2964 (1983); F. F. Abraham, Phys. Rev. Lett. 50, 978 (1983).
[32]J. A. Barker and D. Henderson, Rev. Mod. Phys. 48, 587 (1976); J. A. Barker, P. Henderson, and F. F. Abraham, Physica 106A, 226 (1981).
[33]R. M. J. Cotterill and L. B. Peterson, Solid State Commun. 10, 439 (1972).
[34]D. Frenkel and J. P. McTague, Phys. Rev. Lett. 42, 1632 (1979); J. P. McTague, D. Frenkel, and M. P. Allen, in *Ordering in Two Dimensions,* Ref. 1, p. 147; D. Frenkel, F. E. Hanson, and J. P. McTague, in *Ordering in Strongly Fluctuating Condensed Matter Systems,* Ref. 4, p. 185.
[35]R. C. Gann, S. Chakravarty, and G. V. Chester, Phys. Rev. B 20, 326 (1979).
[36]R. W. Hockney and T. R. Brown, J. Phys. C 8, 1813 (1975).
[37]R. K. Kalia and P. Vashishta, J. Phys. C 14, L643 (1981); R. K. Kalia and P. Vashishta, and S. W. de Leeuw, Phys. Rev B 23, 4794 (1981).
[38]R. H. Morf, Phys. Rev. Lett. 43, 931 (1979).
[39]Y. Saito and H. Muller-Krumbharr, Phys. Rev. B 22, 309 (1981); Y. Saito, *ibid.* 26, 6239 (1982).
[40]P. L. Steinhardt, D. R. Nelson, and M. Ronchetti, Phys. Rev. Lett. 47, 1297 (1981).
[41]F. H. Stillinger and T. A. Weber, J. Chem. Phys. 74, 4015 (1981).
[42]J. Tobochnik and G. V. Chester, Phys. Rev. B 25, 6779 (1982).
[43]S. Toxvaerd, Mol. Phys. 29, 373 (1975); J. Chem. Phys. 69, 4750 (1978); Phys. Rev. Lett. 44, 1002 (1980); Phys. Rev. A 24, 2735 (1981).
[44]F. Tsien and J. P. Valleau, Mol. Phys. 27, 177 (1974).
[45]F. von Swol, L. V. Woodcock, and J. N. Cape, J. Chem. Phys. 73, 913 (1980).
[46]T. A. Weber and F. A. Stillinger, J. Chem. Phys. 74, 4020 (1981).
[47]J. A. Zollweg, in *Ordering in Two Dimensions,* Ref. 1, p. 331.
[48]A. D. Novaco and P. A. Shea, Phys. Rev. B 26, 284 (1982).
[49]C. W. Lemming and G. L. Pollack, Phys. Rev. B 2, 3323 (1970).
[50]M. L. Klein and J. A. Venables, *Rare Gas Solids* (Academic, London, 1976).
[51]C. Tessier, A. Terlain, and Y. Larher, Physica 113A, 286 (1982).
[52]C. F. Prenzlow and G. D. Halsey, J. Phys. Chem. 61, 1158 (1957).
[53]J. R. Sams, G. Constabaris, and G. D. Halsey, J. Phys. Chem. 64, 1689 (1960).
[54]M. C. Cannon, W. R. Grimes, W. T. Ward, and G. M. Watson, Nucl. Sci. Eng. 12, 4 (1962).
[55]H. Cochrane, P. L. Walker, W. S. Diethorn, and H. C. Friedman, J. Colloid. Interface Sci. 24, 405 (1967).
[56]J. Morrison and J. J. Lander, Surf. Sci. 5, 163 (1966); 6, 1 (1967).
[57]A. Thomy and X. Duval, J. Chim. Phys. 66, 1966 (1969); 67, 286, 1101 (1970).
[58]A. Thomy, J. Regnier, J. Menaucourt, and X. Duval, J. Cryst. Growth 13-14, 159 (1972); J. Regnier, A. Thomy, and X. Duval, J. Chim. Phys. 74, 926 (1977).
[59]J. Suzanne, G. Albinet, and M. Bienfait, J. Cryst. Growth 13-14, 164 (1972); 31, 87 (1975); J. Suzanne, J. P. Coulomb, and M. Bienfait, Surf. Sci. 40, 414 (1973); 44, 141 (1974); 47, 204 (1975); J. P. Coulomb, J. Suzanne, M. Bienfait, and P. Masri, Solid State Commun. 15, 1585 (1974).
[60]M. Bienfait and J. A. Venables, Surf. Sci. 64, 425 (1977).
[61]J. A. Venables, H. M. Kramer, and G. L. Price, Surf. Sci. 55, 373 (1976); 57, 782 (1976); 105, 536 (1981); J. A. Venables and P. S. Schabes-Retchkiman, J. Phys. (Paris) Colloq. 38, C4-105 (1977).
[62]G. Quentel, J. M. Richard, and R. Kern, Surf. Sci. 50, 343 (1975).
[63]T. H. Ellis, S. Ianotta, G. Scoles, and U. Valbusa, Phys. Rev. B 24, 2307 (1981).
[64]J. A. Litzinger and G. A. Stewart, in *Ordering in Two Dimensions,* Ref. 1, p. 267.
[65]G. W. Brady, D. B. Fein, and W. A. Steele, Phys. Rev. B 15, 1120 (1977).
[66]E. M. Hammonds, P. A. Heiney, P. W. Stephens, R. J. Birgeneau, and P. M. Horn, J. Phys. C 13, L301 (1980); E. M. Hammonds, M.S. thesis, Massachusetts Institute of Technology, 1980 (unpublished); R. J. Birgeneau, E. M. Hammonds, P. A. Heiney, P. W. Stephens, and P. M. Horn, in *Ordering in Two Dimensions,* Ref. 1, p. 29.
[67]P. A. Heiney, R. J. Birgeneau, G. S. Brown, P. M. Horn, D. E. Moncton, and P. W. Stephens, Phys. Rev. Lett. 48, 104 (1982). P. A. Heiney, Ph.D. thesis, Massachusetts Institute of Technology, 1982 (unpublished).
[68]P. Dutta, S. K. Sinha, and P. Vora, in *Ordering in Two Dimensions,* Ref. 1, p. 169; S. K. Sinha, P. Vora, P. Dutta, and L. Passell, J. Phys. C 15, L275 (1982).
[69]J. P. McTague, J. Als-Nielsen, J. Bohr, and M. Nielsen, Phys. Rev. B 25, 7765 (1982).

[70]P. Dimon, P. M. Horn, M. Sutton, R. J. Birgeneau, and D. E. Moncton (unpublished).
[71]T. F. Rosenbaum, S. E. Nagler, P. M. Horn, and R. Clarke, Phys. Rev. Lett. 50, 1791 (1983).
[72]UCAR-*ZYX* is a product of the Union Carbide Corporation, Carbon Products Division, 270 Park Ave., New York, N.Y.
[73]T. Takaishi and Y. Sensui, Trans. Faraday Soc. 59, 2503 (1962).
[74]S. Brunauer, P. H. Emmett, and E. Teller, J. Am. Chem. Soc. 60, 309 (1938).
[75]D. E. Moncton and G. S. Brown, Nucl. Instrum. Methods 208, 579 (1983).
[76]P. A. Heiney, P. W. Stephens, S. G. J. Mochrie, J. Akimitsu, R. J. Birgeneau, and P. M. Horn, Surf. Sci. 125, 539 (1983); P. W. Stephens, P. A. Heiney, R. J. Birgeneau, P. M. Horn, D. E. Moncton, and G. S. Brown (unpublished).
[77]F. Weling and A. Griffin, Phys. Rev. B 25, 2450 (1982).
[78]P. Dutta and S. K. Sinha, Phys. Rev. Lett. 47, 50 (1981).
[79]M. Abramowitz and I. A. Stegun, *Handbook of Mathematical Functions* (Dover, New York, 1964).
[80]B. E. Warren, Phys. Rev. 59, 693 (1941).
[81]J. K. Kjems, L. Passell, H. Taub, J. G. Dash, and A. D. Novaco, Phys. Rev. B 13, 1446 (1976).
[82]P. W. Stephens, P. A. Heiney, R. J. Birgeneau, and P. M. Horn, Phys. Rev. Lett. 43, 47 (1979).
[83]D. E. Moncton, P. W. Stephens, R. J. Birgeneau, P. M. Horn, and G. S. Brown, Phys. Rev. Lett. 46, 1533 (1981); R. J. Birgeneau, G. S. Brown, P. M. Horn, D. E. Moncton, and P. W. Stephens, J. Phys. C 14, L49 (1981).
[84]R. E. Ecke, J. G. Dash and R. D. Puff, Phys. Rev. B 26, 1288 (1982).
[85]J. M. Greif, D. L. Goodstein, and A. F. Silva-Moreira, Phys. Rev. B 25, 6838 (1982).
[86]J. L. Cardy, Phys. Rev. B 26, 6311 (1982).
[87]D. E. Moncton and R. Pindak, in *Ordering in Two Dimensions,* Ref. 1, p. 83.